

# **Discrete Spring Model for Predicting Delamination Growth in Z-Fiber Reinforced DCB Specimens**

James G. Ratcliffe\* and T. Kevin O'Brien\*\*

\*National Research Council

\*\*U.S. Army Research Laboratory, Vehicle Technology Directorate  
NASA Langley Research Center, Hampton, Virginia, U.S.A

**ABSTRACT:** Beam theory analysis was applied to predict delamination growth in DCB specimens reinforced in the thickness direction with pultruded pins, known as Z-fibers. The specimen arms were modeled as cantilever beams supported by discrete springs, which were included to represent the pins. A bi-linear, irreversible damage law was used to represent Z-fiber damage, the parameters of which were obtained from previous experiments. Closed-form solutions were developed for specimen compliance and displacements corresponding to Z-fiber row locations. A solution strategy was formulated to predict delamination growth, in which the parent laminate mode I critical strain energy release rate was used as the criterion for delamination growth. The solution procedure was coded into FORTRAN 90, giving a dedicated software tool for performing the delamination prediction. Comparison of analysis results with previous analysis and experiment showed good agreement, yielding an initial verification for the analytical procedure.

**KEYWORDS:** Delamination prediction, DCB specimen, strain energy release rate, Simple beam theory, Z-fibers.

### LIST OF SYMBOLS

$a_i$	Distance from spring at location $i$ to beam root.
$a_o$	Length of non-reinforced laminate.
$a_z$	Z-fiber spacing.
$A_p$	Z-fiber cross sectional area.
$b$	DCB Specimen width.
$C$	DCB Specimen compliance.
$d$	Damage parameter.
$E_p$	Z-fiber axial tensile modulus.
$E$	Flexural modulus of DCB specimen arm with no Z-fiber reinforcement.
$E_{zp}$	Flexural modulus of DCB specimen arm with Z-fiber reinforcement.
$F_c$	Critical load for onset of Z-fiber pull-out.
$F_z$	Beam forces in z-axis.
$G$	Strain energy release rate.
$G_{Ic}$	Critical mode-I strain energy release rate.
$h$	DCB specimen arm height.
$I$	Moment of inertia of DCB specimen arm with no Z-fiber reinforcement.
$I_{zp}$	Moment of inertia of DCB specimen arm with Z-fiber reinforcement.
$k_i$	Current Spring stiffness.
$k_o$	Original spring stiffness.
$L$	Total delamination length.
$L_p$	Z-fiber length.
$M$	Bending moment.
$n$	Mode-I compliance calibration exponent.
$P$	Applied load.
$P_c$	Critical load for onset of delamination growth in a DCB specimen.
$r$	Number of Z-fibers per row.

R	Spring reaction load.
U	Stored elastic strain energy.
$z_f$	Z-fiber row displacement at complete pull-out.
$z_i$	Current Z-fiber row displacement.
$z_o$	Z-fiber row displacement at onset of pull-out.
$\Delta$	DCB specimen load-point displacement.
$\Delta$	Mode-I crack length extension factor.
$\Delta_{dev}$	Mode-I crack length extension factor during developing phase of crack growth.
$\Delta_{ss}$	Mode-I crack length extension factor during steady-state phase of crack growth.
$\sigma_c$	Critical stress for onset of Z-fiber pull-out.
$\Delta$	Ratio of Z-fiber spacing to Z-fiber insertion depth.

## INTRODUCTION

A method for enhancing fracture toughness of laminated composite structures uses pins inserted normal to the laminate plane to increase delamination resistance. The pins, known as Z-fibers, are inserted into the prepreg laminate using an ultrasonic hammer prior to the curing process, resulting in a field of pins embedded normal to the laminate plane, as illustrated in Fig.1. A cross section of laminate containing Z-fiber reinforcement is pictured in Fig.2. It can be seen that the reinforcing fibers are not exactly normal to the laminate plane. This is a consequence of the fibers rotating during the insertion process.

The Z-fibers are typically 0.28-mm to 0.5-mm in diameter. Standard areal densities range from 0.5% to 4%. The Z-fibers are provided by the manufacturer, Aztex<sup>®</sup>, in a low-density foam preform, which acts to stabilize orientation of the pins during the insertion process [1-3]. Typical pin materials include boron and carbon fibers embedded in a polymer matrix.

Mode I delamination resistance is enhanced because Z-fibers provide a direct closure traction to the opening of delaminating surfaces. A study of delamination growth in IMS/924 double cantilever beam (DCB) specimens [4], reinforced with carbon/BMI Z-fibers, demonstrated that a significant increase in mode I fracture toughness is achieved as a result of the through thickness reinforcement [5]. It was found that an areal density of 0.5% and 2% Z-fibers resulted in a four-fold and seventeen-fold increase in the non-reinforced fracture toughness of the laminate respectively.

Behavior of delamination growth in DCB specimens containing Z-fibers is defined as a three-phase process in the current work, although others consider it a two-stage process [6-7]. Firstly, the delamination front reaches the Z-fiber field (Stage 1, Fig. 3). Delamination continues through the field of reinforcement, causing Z-fibers to bridge the delamination. Initially, the number of bridging Z-fibers increases as the delamination grows, resulting in an increase in critical fracture load. This is termed the developing growth phase and is labeled Stage 2 in Fig.3. Finally, delamination growth reaches a steady-state, during which a new bridging Z-fiber row is created as another is completely pulled out from the material.

The net effect is a constant number of bridging Z-fiber rows as delamination growth continues. This is termed steady-state growth (Stage 3, Fig.3).

A number of researchers have performed numerical and analytical studies of delamination growth in DCB specimens, reinforced either by stitching or Z-fibers. Jain and Mai [8] developed an analytical model of a stitched DCB specimen, in which the bridging stress provided by the stitches was represented as a distributed load over the bridged zone of the specimen arm. The analyses were used to predict the increase in delamination resistance associated with the through-thickness reinforcement.

During an investigation into the fracture behavior of debonding in integrally stiffened panels, Glaessgen *et al* [9] performed finite element analyses of stitched DCB specimens. In this work, plane stress plate elements were used to represent the skin and stiffener materials, while the stitches were modeled as discrete, nonlinear, fastener elements, the stiffness of which was obtained from experiment. The virtual crack closure technique (VCCT) [10] was used to compute energy release rate values following each analysis. The analysis was used to study the effect of stitching parameters on energy release rate of the reinforced specimen.

Cartié and Partridge [11] performed finite element analyses of unidirectional, carbon fiber/epoxy DCB specimens containing Z-fibers. Plane strain elements were used to represent the laminate material. Single Z-fiber pull-out tests were performed prior to the analyses, to determine the bridging law exhibited by the Z-fibers as they are loaded under mode I conditions. Loading was applied at nodal locations corresponding to the position of each Z-fiber row, in order to represent the bridging action exhibited by the through thickness reinforcement. Load-displacement plots and delamination resistance curves (R-curves) were generated following the analyses.

In [12], Robinson and Das performed DCB tests on IM7/8552 tape laminates with a unidirectional stacking sequence and reinforced with Z-fibers. An analysis similar to [8] was developed to predict delamination growth in the DCB specimens. The analysis was conducted in two parts. First, the developing phase of delamination growth was analyzed. In the second stage of the analysis, delamination growth corresponding to the steady-state phase was predicted. The bridging stresses exhibited by the bridging Z-fibers were modeled as a distributed load along the bridged section of the DCB specimen arms. Following the analysis, compliance calibration and modified beam theory techniques [4] were used to calculate apparent fracture toughness values.

The aim of the current work was to develop an analysis technique capable of predicting delamination growth behavior of DCB specimens reinforced with Z-fibers. The resulting technique modeled specimen arms as cantilever beams with discrete springs used to represent Z-fiber rows. Closed-form solutions were derived for specimen compliance and Z-fiber displacement. The solution procedure was coded into FORTRAN 90, enabling an efficient execution of the analysis. The analysis can be used to study the effect of Z-fiber insert length, areal density and diameter on the apparent fracture toughness of the reinforced specimen. Furthermore, the analysis is coded to enable the use of alternative bridging laws for representing Z-fiber failure. Because Z-fibers are represented using springs, the unstable nature of delamination growth is captured by the analysis, unlike the

analysis of [8, 12], in which the bridging stresses of the Z-fibers are represented as a distributed load. The analysis technique may also be used to design Z-fiber reinforced DCB specimens. Preparation for DCB tests can be eased by using the analysis to estimate the maximum load and displacement that will be experienced during a test.

### **Analysis Procedure for Predicting Delamination Growth in Z-Fiber Reinforced DCB Specimens**

The analysis procedure used for predicting delamination growth in Z-fiber reinforced DCB specimens is comprised of several main steps. First, the specimen was modeled as cantilever beams with springs representing Z-fiber rows. Closed-form solutions for the specimen compliance and displacements were then derived. A damage law was applied to the springs, in order to represent the behavior of Z-fibers as they are removed from the parent laminate during a DCB test. Linear elastic fracture mechanics (LEFM) was used to calculate the strain energy release rate,  $G$ , in the specimen for a given load-point displacement. The value of  $G$  was compared with the critical mode-I strain energy release rate,  $G_{Ic}$ , of the parent laminate material. Delamination growth was assumed to take place when  $G$  became greater than or equal to  $G_{Ic}$ . Finally, a solution strategy was developed to allow delamination growth prediction in a Z-fiber reinforced DCB specimen. The remainder of this section details the five main steps of the analysis. A description of the data reduction schemes that are used to calculate  $G_{Ic}$  from the analysis data is given at the end of the section.

#### *Z-Fiber Reinforced DCB Specimen Model*

Z-fiber reinforced DCB specimens were modeled using cantilever beams to represent the specimen arms. A discrete spring was used for representing each Z-fiber row that may bridge the delamination. Figure 4 illustrates how the 2-dimensional model represents an actual DCB specimen, where three rows of Z-fibers are shown to be bridging the delamination.

#### *Displacement Equations of a Z-Fiber Reinforced DCB Specimen*

Closed-form solutions were derived for the displacement of DCB specimens with delaminations bridged by one, two and three Z-fiber rows. Finally, the solutions were generalized to accommodate for any number of bridging Z-fiber rows.

It was assumed that the upper and lower DCB specimen arms were identical and displacement of each arm was symmetrical about the neutral axis of the specimen, as illustrated in Fig.4. Consequently, a single specimen arm was modeled throughout the analysis. The displacement equations were doubled, yielding an estimate of the total DCB specimen displacements.

A schematic of a specimen arm model with one bridging Z-fiber row is given in Fig.5a. The free body diagram of the arm is given in Fig.5b. Z-fiber rows were

represented by discrete springs positioned normal to the x-y plane. The length of the spring is equivalent to the Z-fiber insertion depth in one arm. Studies have shown that in-plane elastic properties of a laminate may suffer some degradation as a result of the Z-fiber insertion process [13-15]. Consequently, the flexural modulus of the laminate containing Z-fibers was treated separately from that of the remaining laminate. Using the free body diagram in Fig.5b, the equilibrium equations of the arm are:

$$\begin{aligned} \sum F_z = 0 &= P - R_o - \frac{Z_1}{2}(2k_1) & R_o &= P - \frac{Z_1}{2}(2k_1) \\ \sum M = 0 &= PL - M_o - \frac{Z_1}{2}(2k_1)a_1 & M_o &= PL - \frac{Z_1}{2}(2k_1)a_1 \end{aligned} \quad (1)$$

In the above and remaining equilibrium equations, the spring displacements,  $z$ , are halved and the stiffness values,  $k$ , are doubled to accommodate for the fact that half the total Z-fiber length is modeled.

The reaction load,  $R_i$  of a spring at location 'i' was assumed to be in direct proportion to the displacement of the spring in the z-axis,  $z_i$ , by the spring stiffness,  $k_i$  such that:

$$R_i = \frac{Z_i}{2}(2k_i) \quad (2)$$

Following simple beam theory analysis [16], the spring displacement,  $\frac{Z_1}{2}$ , and load-point displacement,  $\frac{\Delta}{2}$  of one half of the DCB specimen were expressed as:

$$\frac{z_1}{2} = \frac{Pa_1^2(3L - a_1)}{6E_{zp}I_{zp} + 2k_1a_1^3} \quad (3)$$

$$\frac{\Delta}{2} = P \left[ \frac{a_o^3}{3EI} + \frac{L^3 - a_o^3}{3E_{zp}I_{zp}} \right] + \frac{k_1 z_1 a_1^2 (a_1 - 3L)}{6E_{zp}I_{zp}} \quad (4)$$

where  $E$  and  $E_{zp}$  are the flexural modulus of the non-reinforced and Z-fiber reinforced sections of the arm respectively. The parameter,  $I$ , is the moment of inertia of the non-reinforced specimen arm and  $I_{zp}$  is the moment of inertia of the specimen arm containing Z-fibers. These moment of inertia values were equal in all cases studied in the current work. The dimension,  $L$ , is the arm length, measured from the loading point to the crack tip and  $a_1$  is the distance between the Z-fiber and crack tip. The parameter  $a_o$  is the length of non-reinforced laminate, where the region of Z-fiber reinforcement was assumed to begin one Z-fiber spacing away from the first Z-fiber row. The load applied to the specimen is denoted as  $P$  and  $k_1$  is the spring stiffness.

Assuming the upper and lower arms of the specimen are identical and the delamination is located at the specimen mid-plane, Eqns.3 and 4 are doubled to

yield the Z-fiber row displacement and load-point displacement of the complete DCB specimen:

$$z_1 = \frac{Pa_1^2(3L - a_1)}{3E_{zp}I_{zp} + k_1a_1^3} \quad (5)$$

$$\delta_1 = 2P \frac{\delta_0^3}{3EI} + \frac{L^3 - \delta_0^3}{3E_{zp}I_{zp}} + \frac{k_1z_1a_1^2(a_1 - 3L)}{3E_{zp}I_{zp}} \quad (6)$$

The subscript on the left-hand side of Eqn.5 indicates displacement of the specimen at a distance,  $a_1$ , from the arm root, as illustrated in Fig.5a. The subscript on the left-hand side of Eqn.6 represents the number of Z-fiber rows bridging the specimen.

Specimen compliance,  $C$ , is calculated by dividing the load-point displacement by the applied load,  $P$ . Therefore, compliance of the DCB specimen with a single bridging Z-fiber is found from Eqn.6:

$$C_1 = \frac{\delta_1}{P} = 2 \frac{\delta_0^3}{3EI} + \frac{L^3 - \delta_0^3}{3E_{zp}I_{zp}} + \frac{k_1z_1a_1^2(a_1 - 3L)}{3PE_{zp}I_{zp}} \quad (7)$$

Again, the subscript on the left-hand side of Eqn.7 refers to the number of bridging Z-fiber rows.

The analysis is now extended to calculate the displacements of a DCB specimen, in which the delamination is bridged by two Z-fiber rows. Figure 6a illustrates the specimen arm. A free body diagram of the arm is also shown in the figure. The equilibrium equations of the arm are:

$$\sum F_z = 0 = P - R_o - \frac{z_1}{2}(2k_1) - \frac{z_2}{2}(2k_2) \quad \sum R_o = P - \frac{z_1}{2}(2k_1) - \frac{z_2}{2}(2k_2) \quad (8)$$

$$\sum M = 0 = PL - M_o - \frac{z_1}{2}(2k_1)a_1 - \frac{z_2}{2}(2k_2)a_2 \quad \sum M_o = PL - \frac{z_1}{2}(2k_1)a_1 - \frac{z_2}{2}(2k_2)a_2$$

Beam theory analysis leads to solutions for the Z-fiber row displacements\*,  $z_1$  and  $z_2$ , at locations 1 and 2 respectively along the beam.

$$z_1 = \frac{Pa_1^2(3L - a_1) + z_2k_2a_1^2(a_1 - 3a_2)}{3E_{zp}I_{zp} + k_1a_1^3} \quad (9)$$

$$z_2 = \frac{Pa_2^2(3L - a_2) + z_1k_1a_1^2(a_1 - 3a_2)}{3E_{zp}I_{zp} + k_2a_2^3} \quad (10)$$

\* [The remaining solutions are doubled to reflect displacements and compliance of the entire DCB specimen.](#)

Compliance of a DCB specimen with two bridging Z-fiber rows is:

$$C_2 = \frac{\delta_2}{P} = 2 \frac{\delta_0^3}{3EI} + \frac{L^3 \delta_0^3}{3E_{zp} I_{zp}} + \frac{\delta_0 [k_1 z_1 a_1^2 (a_1 - 3L) + k_2 z_2 a_2^2 (a_2 - 3L)]}{3PE_{zp} I_{zp}} \quad (11)$$

The schematic of a specimen arm bridged by three Z-fiber rows is given in Fig.6b. The free body diagram of the arm is also shown and the corresponding equilibrium equations are:

$$\begin{aligned} \sum F_z = 0 &= P - R_o - \frac{z_1}{2}(2k_1) - \frac{z_2}{2}(2k_2) - \frac{z_3}{2}(2k_3) \\ \sum R_o &= P - \left[ \frac{z_1}{2}(2k_1) + \frac{z_2}{2}(2k_2) + \frac{z_3}{2}(2k_3) \right] \\ \sum M = 0 &= PL - M_o - \frac{z_1}{2}(2k_1)a_1 - \frac{z_2}{2}(2k_2)a_2 - \frac{z_3}{2}(2k_3)a_3 \\ \sum M_o &= PL - \left[ \frac{z_1}{2}(2k_1)a_1 + \frac{z_2}{2}(2k_2)a_2 + \frac{z_3}{2}(2k_3)a_3 \right] \end{aligned} \quad (12)$$

Z-fiber row displacements,  $z_1$ ,  $z_2$  and  $z_3$ , at locations 1, 2 and 3 respectively along the beam are:

$$z_1 = \frac{Pa_1^2(3L - a_1) + z_2 k_2 a_1^2 (a_1 - 3a_2) + z_3 k_3 a_1^2 (a_1 - 3a_3)}{3E_{zp} I_{zp} + k_1 a_1^3} \quad (13)$$

$$z_2 = \frac{Pa_2^2(3L - a_2) + z_1 k_1 a_1^2 (a_1 - 3a_2) + z_3 k_3 a_2^2 (a_2 - 3a_3)}{3E_{zp} I_{zp} + k_2 a_2^3} \quad (14)$$

$$z_3 = \frac{Pa_3^2(3L - a_3) + z_1 k_1 a_1^2 (a_1 - 3a_3) + z_2 k_2 a_2^2 (a_2 - 3a_3)}{3E_{zp} I_{zp} + k_3 a_3^3} \quad (15)$$

Compliance of the DCB specimen with three bridging Z-fiber rows is:

$$C_3 = \frac{\delta_3}{P} = 2 \frac{\delta_0^3}{3EI} + \frac{L^3 \delta_0^3}{3E_{zp} I_{zp}} + \frac{\delta_0 [k_1 z_1 a_1^2 (a_1 - 3L) + k_2 z_2 a_2^2 (a_2 - 3L) + k_3 z_3 a_3^2 (a_3 - 3L)]}{3PE_{zp} I_{zp}} \quad (16)$$

The analysis is extended to included any number of Z-fiber rows bridging the delamination of the DCB specimen. Figure 6c shows one arm of a DCB specimen bridged by an arbitrary number of Z-fiber rows,  $n$ . The free body diagram of the arm is also given in Fig.6c. Following the diagram, the equilibrium equations for the arm are:

$$\sum F_z = 0 = P \sum R_o \sum_{i=1}^n \frac{Z_i}{2} (2k_i) \quad \sum R_o = P \sum_{i=1}^n \frac{Z_i}{2} (2k_i) \quad (17)$$

$$\sum M = 0 = PL \sum M_o \sum_{i=1}^n \frac{Z_i}{2} (2k_i) a_i \quad \sum M_o = PL \sum_{i=1}^n \frac{Z_i}{2} (2k_i) a_i$$

Displacements in the z direction, corresponding to each Z-fiber row location in the DCB specimen are:

$$\begin{aligned} z_1 &= \frac{1}{3E_{zp}I_{zp} + k_1a_1^3} \left[ Pa_1^2(3L - a_1) + z_2k_2a_1^2(a_1 - 3a_2) + z_3k_3a_1^2(a_1 - 3a_3) + \dots \right. \\ &\quad \left. + z_{n-1}k_{n-1}a_1^2(a_1 - 3a_{n-1}) + z_nk_na_1^2(a_1 - 3a_n) \right] \\ z_2 &= \frac{1}{3E_{zp}I_{zp} + k_2a_2^3} \left[ Pa_2^2(3L - a_2) + z_1k_1a_2^2(a_1 - 3a_2) + z_3k_3a_2^2(a_2 - 3a_3) + \dots \right. \\ &\quad \left. + z_{n-1}k_{n-1}a_2^2(a_2 - 3a_{n-1}) + z_nk_na_2^2(a_2 - 3a_n) \right] \\ z_3 &= \frac{1}{3E_{zp}I_{zp} + k_3a_3^3} \left[ Pa_3^2(3L - a_3) + z_1k_1a_3^2(a_1 - 3a_3) + z_2k_2a_3^2(a_2 - 3a_3) + \dots \right. \\ &\quad \left. + z_{n-1}k_{n-1}a_3^2(a_3 - 3a_{n-1}) + z_nk_na_3^2(a_3 - 3a_n) \right] \\ z_{n-1} &= \frac{1}{3E_{zp}I_{zp} + k_{n-1}a_{n-1}^3} \left[ Pa_{n-1}^2(3L - a_{n-1}) + z_1k_1a_{n-1}^2(a_1 - 3a_{n-1}) + z_2k_2a_{n-1}^2(a_2 - 3a_{n-1}) \right. \\ &\quad \left. + z_3k_3a_{n-1}^2(a_3 - 3a_{n-1}) + \dots + z_nk_na_{n-1}^2(a_{n-1} - 3a_n) \right] \\ z_n &= \frac{1}{3E_{zp}I_{zp} + k_na_n^3} \left[ Pa_n^2(3L - a_n) + z_1k_1a_n^2(a_1 - 3a_n) + z_2k_2a_n^2(a_2 - 3a_n) \right. \\ &\quad \left. + z_3k_3a_n^2(a_3 - 3a_n) + \dots + z_{n-1}k_{n-1}a_n^2(a_{n-1} - 3a_n) \right] \end{aligned} \quad (18)$$

The displacements are solved simultaneously, yielding the solutions for each Z-fiber row displacement.

Compliance of the DCB specimen bridged by any number, n, Z-fiber rows is given by:

$$C_n = \frac{\sum z_i}{P} = 2 \sum_{i=1}^n \frac{a_o^3}{3EI} + \frac{L^3 \sum_{i=1}^n a_o^3}{3E_{zp}I_{zp}} + \frac{1}{3PE_{zp}I_{zp}} \sum_{i=1}^n k_i z_i a_i^2 (a_i - 3L) \quad (19)$$

### Z-Fiber Pull-out Bridging Law

A bi-linear, softening constitutive model [17] was used to represent the damage incurred in Z-fiber rows, as they pull from the laminate during a DCB test. A typical illustration of the history from a Z-fiber pull-out test is illustrated in Fig. 7. Upon initial loading, the Z-fiber row exhibits a constant stiffness, until a critical displacement,  $z_o$ , is achieved, after which the stiffness decreases linearly with displacement. Load-displacement responses following pull-out tests on single Z-fibers have exhibited similar damage behavior [11, 12].

Using this damage model, the stiffness of the Z-fibers is calculated according to the following conditions (Fig. 7):

$$k_i = \begin{cases} k_o & \text{if } z_i \leq z_o \\ (1-d)k_o & \text{if } z_o < z_i < z_f \\ 0 & \text{if } z_i \geq z_f \end{cases} \quad (20)$$

where  $z_o$  is the Z-fiber row displacement corresponding to the onset of damage,  $z_f$  is the displacement at which the Z-fiber row stiffness becomes zero, corresponding to complete pull out. It is usual for Z-fibers to be removed from one side of the DCB specimen only. Therefore,  $z_f$  is assumed to be half the total Z-fiber insert length. The damage parameter,  $d$ , is given by [16]:

$$d = \frac{z_f(z_i - z_o)}{z_i(z_f - z_o)} \quad (21)$$

The initial Z-fiber row stiffness,  $k_o$ , is calculated using the following relation:

$$k_o = r \frac{E_p A_p}{L_p} \quad (22)$$

where  $E_p$ ,  $A_p$  and  $L_p$  are the axial tensile modulus, cross sectional area and length of a single Z-fiber respectively.  $r$  is the number of Z-fibers per row.

The Z-fiber row displacement corresponding to the onset of damage,  $z_o$ , is calculated from the row stiffness,  $k_o$ , and the peak load,  $F_c$ , measured from a single Z-fiber pull out test, (Fig. 7) such that:

$$z_o = r \frac{F_c}{k_o} \quad (23)$$

The Z-fiber displacement corresponding to complete removal from the specimen,  $z_f$ , is equal to the insertion depth into one of the DCB specimen arms.

### *Strain Energy Release Rate Calculation*

Strain energy release rate values were calculated by repeating an analysis of a DCB specimen containing delaminations of neighboring lengths, as illustrated in Fig.8a. The same load-point displacement,  $d$ , is applied in both analyses. The strain energy,  $U_1$ , stored in the specimen with delamination of length  $L_1$  is equal to the area OAC under the load-displacement plot illustrated in Fig.8b. The stored elastic strain energy,  $U_2$ , in the specimen with the neighboring delamination of length,  $L_2$  is given by the area OBC under the load-displacement plot in Fig.8b. Therefore, the strain energy release rate,  $G$ , for delamination growth from  $L_1$  to  $L_2$  is given as:

$$G = \frac{1}{b} \frac{dU}{dL} = \frac{1}{b} \frac{U_1 - U_2}{L_2 - L_1} \quad (24)$$

where  $b$  is the DCB specimen width.

The strain energy release rate for a delamination length of  $L_1$  is estimated from Eqn.24. This calculation of  $G$  becomes more accurate as the difference between neighboring delamination lengths,  $L_1$  and  $L_2$ , decreases. Consequently, a convergence study was undertaken to determine the value of  $(L_2-L_1)$  required to yield accurate strain energy release rate estimates. This study is detailed in the model verification section.

### *Delamination Growth Solution Strategy*

A strategy was formulated to apply the analysis detailed above, enabling prediction of delamination growth through a Z-fiber reinforced DCB specimen.

Firstly, the specimen configuration is prescribed, including specimen dimensions, elastic properties, areal density of Z-fibers, number of Z-fiber rows and Z-fiber insertion length. An initial load-point displacement,  $\Delta$ , is applied and the corresponding specimen compliance is calculated. The following relation is then used to determine the applied load,  $P$ :

$$P = \frac{\Delta}{C} \quad (25)$$

The applied load,  $P$ , is then used to calculate the Z-fiber row displacements. If more than one row bridges the delamination, Gaussian elimination with partial pivoting is used to solve the simultaneous equations. The method described previously is then used to calculate the strain energy release rate corresponding to the displacement increment. This value is then compared with the critical mode I strain energy release rate,  $G_{Ic}$ , of the parent laminate. Delamination is assumed to occur when  $G = G_{Ic}$  and thus a new delamination length increment is chosen at this stage. If  $G < G_{Ic}$ , the displacement increment is repeated using a larger value of load-point displacement. Once a Z-fiber row displacement reaches the critical value for damage onset,  $z_o$ , the bi-linear bridging law is implemented to adjust the Z-fiber row stiffness. During this stage of the solution procedure, each displacement increment is repeated with the updated Z-fiber row stiffness values until no further change in stiffness is incurred within that displacement increment. Once equilibrium of the row stiffness values has been achieved, the energy release rate calculations are performed and the remainder of the analysis continues. A flow chart summarizing the solution procedure, as implemented into the FORTRAN 90 code, is presented in Fig.9.

### *Data Reduction Schemes*

The load-point displacement, applied load and corresponding delamination lengths calculated from the analysis are reduced in a similar manner to data obtained from an actual DCB test. Compliance calibration and modified beam theory data reduction schemes [4] were selected for calculating an effective fracture toughness of the Z-fiber reinforced DCB specimen. The corresponding expressions for fracture toughness using the compliance calibration and modified beam theory methods are given in Eqn. 26 [4].

$$\begin{aligned}
G_{Ic} &= \frac{nP_c \Delta_c}{2bL} && \text{(Compliance calibration)} \\
G_{Ic} &= \frac{3P_c \Delta_c}{2b(L + \Delta)} && \text{(Modified beam theory)}
\end{aligned}
\tag{26}$$

where  $P_c$  and  $\Delta_c$  are the critical load and displacement respectively for the onset of delamination growth.

These data reduction schemes require that the term,  $n$ , is determined as the slope from a plot of the log of compliance versus log of load-point displacement. A crack length extension factor,  $\Delta$ , is determined as the intercept from a plot of the cube root of compliance versus delamination length.

### **Model Verification**

Verification of the current modeling approach was undertaken in four stages. Firstly, a convergence study was conducted on the method for calculating strain energy release rate values using Eqn.24. The current analysis was used to model two independent specimen configurations available in the literature. Finally, a series of analyses were conducted to demonstrate that the current analysis captures unstable delamination growth, when the spacing of Z-fiber rows is sufficiently large.

#### *Convergence Study on Non-reinforced DCB Specimen [18]*

A convergence study was conducted to determine the difference in neighboring delamination lengths,  $dL$ , required to yield accurate strain energy release rate values, as calculated using Eqn.24. The DCB specimen discussed in [18] was used in the convergence study. The specimen contained no Z-fiber reinforcement. Other specimen details are presented in Table 1. Critical load and load-point displacement values were estimated for delamination lengths of 50-mm and 99-mm. The analyses were repeated using different values of  $dL$ . The estimated critical load and displacement values for delamination growth were normalized by the corresponding experimental values and plotted as a function of  $dL$ /delamination length,  $L$ . The results indicate that neighboring analyses differ by less than one percent once the difference in neighboring delamination lengths is equal to or less than 0.2% of the delamination length,  $L_1$ . The results for the 50-mm and 99-mm cases are presented in Figs. 10a and 10b respectively. In both cases convergence is assumed when  $dL/L \leq 2 \times 10^{-3}$ , and therefore this value of  $dL$  was used for the difference in neighboring crack lengths. To ensure convergence was achieved during analysis of Z-fiber reinforced DCB specimens, the difference in neighboring delamination length was set to 0.1% of the Z-fiber spacing.

### *Analysis of Z-Fiber Reinforced IM7/8552 DCB Specimens [12]*

Robinson and Das [12] conducted DCB tests on specimens manufactured from IM7/8552 tape laminate with a stacking sequence of  $[0]_{48}$ , yielding a specimen arm thickness of 3-mm. A field of carbon/BMI Z-fibers was inserted into the DCB specimens as illustrated in Fig.11. Z-fibers were placed at 2-mm intervals, giving an areal density of 1.5%. An analysis method was used to predict delamination growth in the DCB specimens. Critical strain energy release rates were calculated using the data reduction schemes described earlier.

The load displacement responses, predicted following the original and current analyses, are presented in Fig.12 and show reasonable agreement. Data reduction from the current analysis was carried out in order to calculate an apparent toughness of the specimen. Compliance calibration and modified beam theory plots from the current analysis data are presented in Figs.13 and 14 respectively. Both curves exhibit linear regions that correspond to the developing and steady-state phases of delamination growth, as indicated in the figures. The steady-state phase of delamination growth yielded the highest value of the exponent,  $n$ , and the lowest crack length correction factor,  $\Delta$ , in comparison to the developing stage. Similar observations were made by Robinson and Das [12]. Compliance calibration and modified beam theory were used to calculate the apparent fracture toughness and were found to produce similar toughness values. A plot of the R-curve as predicted from the current analysis is presented in Fig.15. Also in the figure is the R-curve prediction from the original analysis [12]. The toughness values shown from the current analysis were calculated using the compliance calibration method, and a value of  $n = 3.19$ .

Predictions from the two analyses agree well. However, the data reduction schemes, which were developed for non-reinforced laminates may produce invalid global toughness values because the damage zone is significant relative to the specimen dimensions (as the damage zone spans the bridging Z-fibers being removed from the specimen) and in the developing stage, delamination growth is not self-similar. Because self-similar delamination occurs only during the steady-state phase of delamination growth (when the number of bridging Z-fibers is constant), only the data corresponding to this delamination stage is recommended for use with existing data reduction schemes. Similar recommendations were made by Robinson and Das [12].

### *Analysis of Z-Fiber Reinforced IMS/924 DCB Specimens [18]*

The current analysis technique was used to model DCB tests conducted by Cartié [18] on IMS/924 carbon tape specimens with a unidirectional stacking sequence, reinforced with carbon/BMI Z-fibers. A specimen configuration containing 0.5% areal density and one containing 2% areal density of Z-fibers was modeled, details of which are presented in Tables 3 and 4 respectively. The bridging law for each case was obtained from single Z-fiber pull-out tests [18].

The load displacement response estimated from the analysis of both specimen types is given in Figs. 16 and 17 respectively. A comparison with the experimental load displacement traces is given for each case and shows a

reasonable agreement between experiment and analysis in the 0.5% areal density case (Fig.16). The developing section of the load displacement traces in the 2% areal density case calculated from the analysis does not agree well with the experiment. This disagreement, however, does reduce in the steady-state stage of delamination growth (Fig.17). A selection of delamination lengths corresponding to the analytical load-displacement traces is also given. Figures 18 and 19 present plots of the load-point displacement versus delamination length from the analysis and corresponding experiment for the 0.5% and 2% areal density cases respectively. The first case shows good agreement with experiment (Fig.18), indicating the analysis yields a reasonable prediction for delamination growth. In the 2% areal density case (Fig.19), the analytical displacement versus delamination length curve only agrees with experiment after steady-state growth has been reached. The disparity is likely due to the assumptions made in the analysis and the variability of the Z-fiber region in the experiment, as parameters such as insertion depth and angle of Z-fibers have been shown to greatly affect the resulting delamination response of DCB specimens [5]. Furthermore, uneven delamination growth is likely to take place, which will influence the delamination length readings taken during the experiment. This disparity in load-point displacement versus delamination length curves may also explain the difference in the developing regions of the load displacement traces from analysis and experiment for the 2% areal density case.

Again, the compliance calibration and modified beam theory techniques were used to reduce the analytical data. Consider first the compliance calibration plots from analyses of both specimens shown in Fig.20. In accordance with the previous example, the steady-state phase of growth yields the highest values of  $n$ . The corresponding modified beam theory curves for both specimens are given in Fig.21. Again, the values of crack length extension factor are highest during the developing stage of delamination growth. A summary of the findings from the compliance calibration and modified beam theory plots are given in Figs.20 and 21.

Because the developing phase of delamination growth is not self-similar, the apparent fracture toughness was calculated for the steady-state phase only. The experimental data corresponding to the steady-state phase of delamination was used in the current work with the compliance calibration technique for calculating the experimental values of  $G_{Ic}$ . Figure 22 presents the experimental compliance calibration curves for the 0.5% and 2% areal density cases. A summary of the resulting values of the exponent,  $n$ , is also given in the figure and shows the same trends as determined through the analysis. The values corresponding to steady-state delamination were used in the data reduction for calculating the experimental values of  $G_{Ic}$ . The R-curves from the analyses for the 0.5% and 2% areal density cases are given in Figs. 23 and 24 respectively. There is reasonable agreement between the analytical and experimental values. The average experimental steady-state value of  $G_{Ic}$  for the 0.5% areal density specimen was 1457-N/m. The corresponding analytical value was 1390-N/m, corresponding to a 5% error between experiment and analysis. The average experimental steady-state value of  $G_{Ic}$  for the 2% areal density specimen was 5847-N/m and the corresponding analytical value was 5342-N/m. The error between experiment and analysis for this case was 10%.

## *The Effect of Z-Fiber Row Spacing on Delamination Growth Behavior*

If the spacing of Z-fiber rows in the direction of delamination growth is small, the direct closure traction provided by the bridging fibers will be similar to a distributed load across the bridged region of the DCB specimen. Consequently, steady-state delamination growth will be stable with respect to load-point displacement. However, as Z-fiber row spacing increases, the bridging stresses will become discrete and the resulting steady-state delamination will be unstable. To test the ability of the current analysis to capture this change in delamination behavior with Z-fiber row spacing, a DCB specimen analysis was performed for the specimen detailed in Fig.25a, in which the Z-fiber spacing was 1.5-mm (spacing to Z-fiber insertion depth ratio,  $w=1.5/2=0.75$ ). The analysis was repeated for the same specimen but using a Z-fiber spacing of 5-mm ( $w=2.5$ ). In order to provide a direct comparison of delamination behavior between the two cases, the peak stress for the onset of Z-fiber pull-out was kept constant. This was achieved in the following manner:

The assumed bridging law for the case of a Z-fiber row spacing of 1.5-mm is summarized in Fig.25b. The critical stress corresponding to the onset of Z-fiber pull-out,  $\sigma_c$ , is given by the critical load divided by the area of a unit-cell containing one Z-fiber [12] (Fig.25a):

$$\sigma_c = \frac{F_c}{a_z^2} \quad (27)$$

Thus, for the 1.5-mm Z-fiber spacing example, the critical stress for the onset of Z-fiber pull-out was  $3.4\text{N}/(1.5\text{mm})^2=1.51\text{N}/\text{mm}^2$ .

The critical stress for the 5-mm Z-fiber spacing example was kept equal to  $1.51\text{N}/\text{mm}^2$  by factoring the original critical load,  $F_c$ , by the ratio of the area of the 5-mm square unit-cell and the 1.5-mm square unit cell, such that:

$$F_c = 3.4 \frac{5^2}{1.5^2} = 37.78\text{N} \quad (28)$$

The resulting Z-fiber pull-out bridging law for the 5-mm spacing example is given in Fig.25c.

Load displacement plots from analyses of the 1.5-mm and 5-mm Z-fiber spacing models are given in Fig.26. The values of load and displacement from both cases are expected to be the same because the critical load for the onset of Z-fiber pull-out was adjusted to keep the critical stress values the same. As expected, the load displacement response corresponding to the 5-mm spacing consists of sudden load drops. This is in contrast to the stable response from the example with the smaller spacing. The corresponding load-point displacement versus delamination length curves are presented in Fig.27. In the 5-mm spacing example, steady-state delamination growth occurs via discrete increases for little change in displacement. This confirms that the sudden load drops in the load displacement response do correspond to unstable delamination growth.

This study demonstrates that the current analysis method is able to capture the discrete delamination growth behavior of Z-fiber reinforced DCB specimens. The study also suggests that the representation of bridging stresses by a distributed load becomes less valid when the Z-fiber spacing is significantly larger than the insertion depth of the reinforcement. In this example significant unstable delamination growth was detected when the Z-fiber spacing was 250% of the insert depth of the Z-fibers.

## **Discussion**

An initial verification of the current analysis for predicting delamination growth in Z-fiber reinforced DCB specimens has been conducted. Comparison of data from current analysis and a previous analysis from [12] shows good agreement. This study indicated that the use of current data reduction schemes intended for non-reinforced DCB specimens is invalid when the specimens contain Z-fiber reinforcement. This is because delamination growth during the developing stage is not self-similar, as the number of bridging Z-fibers increases with delamination length. The steady-state phase of delamination, however, is self-similar, because the number of bridging Z-fibers is constant with delamination length. Subsequently, only data from this stage of delamination growth is recommended for use with current data reduction strategies. Similar conclusions were drawn in the study of [12]. This strategy for data reduction was applied to experimental data from [18] and corresponding analyses were undertaken. The resulting comparison between the current analysis and experiment is acceptable, although there is some scatter in the experimental compliance calibration curves. However, the experimental data exhibited the same trends as the analysis results, in that the exponent,  $n$ , corresponding to steady-state delaminating growth was larger than the developing stage value.

The Z-fiber spacing study demonstrated that the current analysis is able to capture unstable delamination growth, which in this instance occurs when the spacing of Z-fiber rows is greater than the insertion depth of the Z-fibers.

The studies undertaken using the current analysis have provided an initial verification of the accuracy of the analytical method. The analysis, however, does suffer a small number of limitations, such as the inability for representing a Z-fiber insertion angle different from 90 degrees to the laminate plane. The analysis does not accommodate for displacement of the DCB specimen arms due to shear, which will become significant in specimens with thick arms. The analysis is also limited by the assumption made in the beam theory that the beam displacements are small relative to the span. The accuracy of the analysis is also limited by the accuracy of the empirical damage law used to represent Z-fiber failure. However, the current analysis exhibits good agreement with experimental and analytical data from previous work [12, 18].

## Concluding Remarks

Simple beam theory was used to derive closed-form solutions for the displacements and compliance of DCB specimens reinforced with through thickness reinforcement known as Z-fibers. The Z-fibers were represented using discrete springs and a bi-linear cohesive damage law was used to represent Z-fiber failure as they are pulled out from a DCB specimen during testing. The closed-form solutions were used to calculate the rate of change of specimen compliance with delamination length. Linear elastic fracture mechanics was then used to calculate the strain energy release rate. Delamination growth was assumed to take place when the strain energy release rate became equal to the critical strain energy release rate of the parent laminate material. The analysis was coded in FORTRAN 90, yielding a dedicated analysis tool. Initial verification of the analysis was undertaken by comparing data from the analysis with experimental data from the literature. Agreement between analysis and experiment was good. Data from the analysis was also compared with that of a previous analysis for predicting delamination growth in Z-fiber reinforced DCB specimens. Agreement between the current and original analysis methods was very good. Finally, it was found that current data reduction strategies used for calculating  $G_{Ic}$  [4] are only valid during steady-state delamination growth in the Z-fiber reinforced DCB specimens.

## References

1. Freitas, G., Magee, C., Boyce, J., and Bott, R., "Service Tough Composite Structures Using the Z-Direction Reinforcement Process," Proceedings of the 9<sup>th</sup> DoD/NASA/FAA Conference on Fibrous Composites in Structural Design, Lake Tahoe, Nevada, USA, November 1991, NASA-CR-198718.
2. Childress, J.J., and Freitas, G., "Z-direction Pinning of Composite Laminates for Increased Survivability," Proceedings of the AIAA Aerospace Design Conference, Irvine, California, USA, February 1992, paper 92-1099.
3. Freitas, G., Magee, C., Dardsinski, P., and Fusco, T., "Fiber Insertion process for Improved Damage Tolerance in Aircraft Laminates," *Journal of Advanced Materials*, vol.24, July 1994, pp.36-43.
4. ASTM Test Method D 5528-01, "Standard Test Method For Interlaminar Fracture Toughness of Unidirectional Fiber-Reinforced Polymer Matrix Composites," *Annual Book of ASTM Standards*, vol. 15.03, American Society for Testing and Materials, March 2001, West Conshohocken, PA, USA.
5. Cartié, D.D.R., and Partridge, I.K., "Z-Pinning Composite Laminates – Improvements In Delamination Resistance," Proceedings of the Fifth International Conference on Deformation and fracture of Composites, London, UK, March 1999, pp.53-59.
6. Cartié, D.D.R., and Partridge, I.K., "Delamination Behaviour of Z-pinned laminates," Proceedings of the Twelfth International Conference on Composite Materials, Paris, France, July 1999, pp.53-59.
7. Troulis, M., Cartié, D.D.R., Barratoni, L., and Partridge, I.K., "Z-Pinned Woven Laminates: Interlaminar Fracture Results and Pinning Quality Considerations," Proceedings of the Sixth International Conference on Deformation and fracture of Composites, Manchester, UK, April 2001, pp.447-454.
8. Jain, L.K., and Mai, Y-W., "On the Effect of Stitching on Mode I Delamination Toughness of Laminated Composites," *Composites Science and Technology*, vol. 51, 1994, pp.331-345

9. Glaessgen, E.H., Raju, I.S., and Poe, C.C., Jr., "Fracture mechanics Analysis of Stitched Stiffener-Skin Debonding," Proceedings of the AIAA/ASME/ASCE/AHS/ASC Thirty-Ninth Structures, Structural Dynamics and Materials Conference, Long Beach, California, USA, 1998, paper 98-2022.
10. Rybicki, E.F., and Kanninen, M.F., "A Finite Element Calculation of Stress Intensity Factors by a Modified Crack Closure Integral," *Engineering Fracture Mechanics*, Vol.9, 1977, pp.931-938.
11. Cartié, D.D.R., and Partridge, I.K., "A Finite Element Tool For Parametric Studies of Delamination In Z-Pinned Laminates," Proceedings of the Sixth International Conference on Deformation and Fracture of Composites, Manchester, UK, April 2001, pp.49-55.
12. Robinson, P., and Das, S., "Mode I DCB Testing of Z-Fiber Reinforced Laminates: A Simple Model for the Investigation of Data Reduction Strategies," *Journal of Engineering Fracture Mechanics*, Vol. 71, No. 3, 2004, pp. 345-364.
13. Steeves, C.A., PhD Thesis. Department of Engineering, University of Cambridge, UK, 2000.
14. Dickinson, L.C., Farley, G.L., and Hinders, M.K., "Prediction of Effective Three-Dimensional Elastic Constants of Translaminar Reinforced Composites," *Journal of Composite Materials*, vol. 33, 1999, pp.1002-1029.
15. Grassi, M., Zhang, X., and Meo, M., "Prediction of Stiffness and Stresses in Z-fibre Reinforced Composite Laminates," Proceedings of the Sixth International Conference on Deformation and Fracture of Composites, Manchester, UK, April 2001, pp.335-345.
16. Timoshenko, S.P., and Goodier, J.N., "Theory of Elasticity," 3<sup>rd</sup> ed. McGraw-Hill, 1970.
17. Chen, J., Crisfield, M.A., Kinloch, E.P., Busso, E.P., Matthews, F.L. and Qiu, Y., "Predicting Progressive Delamination of Composite Material Specimens Via Interface Elements," *Mechanics of Composite Materials and Structures*, Vol.6, 1999, pp.301-317.
18. Cartié, D.D.R., PhD Thesis. Cranfield College of Aeronautics, Cranfield University, UK, 2001.

TABLE 1. Details [18] of DCB specimen modeled in convergence study.

Arm height [mm], h	1.61
Specimen width [mm], b	20.05
Insert length [mm], $a_p$	49.6
Flexural modulus [ $\text{N/mm}^2$ ], E	125500

TABLE 2. Input data used in analysis of IM7/8552 based DCB specimen [12].

Laminate Details		Z-fiber Details		Bridging Law	
Arm height, h	3mm	Diameter	0.28mm	$z_o$	0.007mm
Width, b	18mm	Length	4mm	$z_f$	2mm
Insert length	73mm	Axial modulus	227GPa	$k_o$	31446N/mm
$E_p=E_{zp}$	160GPa	Spacing	2mm		
$G_{Ic}$	110J/m <sup>2</sup>	Areal density	1.5%		

TABLE 3. Input data used in analysis of IMS/924 based DCB specimen with 0.5% areal density of Z-fibers [18].

Laminate Details		Z-fiber Details		Bridging Law	
Arm height, h	1.615mm	Diameter	0.28mm	$z_o$	$4.4 \times 10^{-3}$ mm
Width, b	20mm	Length	3.23mm	$z_f$	1.615mm
Insert length, $a_o$	50.7mm	Axial modulus	227GPa	$k_o$	21638N/mm
Arm length to Z-fiber region	53.7mm	Spacing	3.5mm		
$E_p=E_{zp}$	126GPa	Z-fibers / row	5		
$G_{Ic}$	268J/m <sup>2</sup>	No of rows	8		
		Areal density	0.5%		

TABLE 4. Input data used in analysis of IMS/924 based DCB specimen with 2% areal density of Z-fibers [18].

Laminate Details		Z-fiber Details		Bridging Law	
Arm height, h	1.63mm	Diameter	0.28mm	$z_o$	$4.4 \times 10^{-3}$ mm
Width, b	20mm	Length	3.26mm	$z_f$	1.63mm
Insert length, $a_o$	50.2mm	Axial modulus	227GPa	$k_o$	47165N/mm
Arm length to Z-fiber region, $a_p$	51.6mm	Spacing	1.8mm		
$E_p=E_{zp}$	126GPa	Z-fibers / row	11		
$G_{Ic}$	268J/m <sup>2</sup>	No of rows	16		
		Areal density	2%		

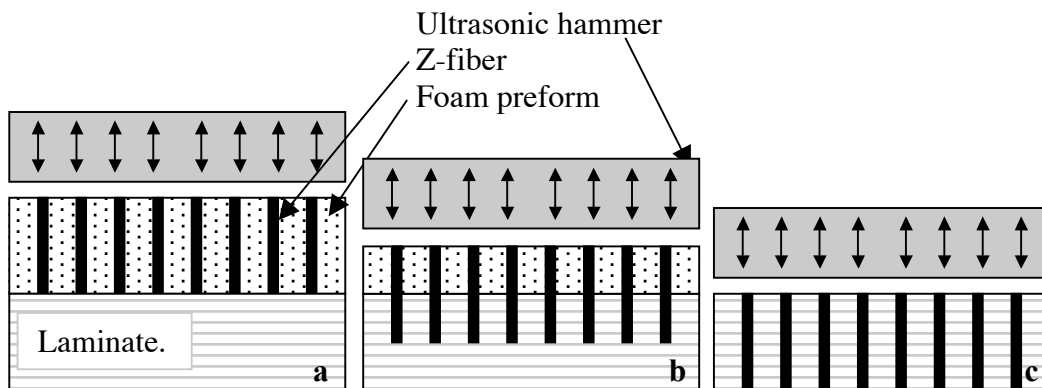


FIGURE 1. (a) Z-fibers held in foam preform positioned on laminate. (b) Ultrasonic hammer drives Z-fibers into laminate. (c) Completion of Z-fiber insertion. Preform material removed during insertion.

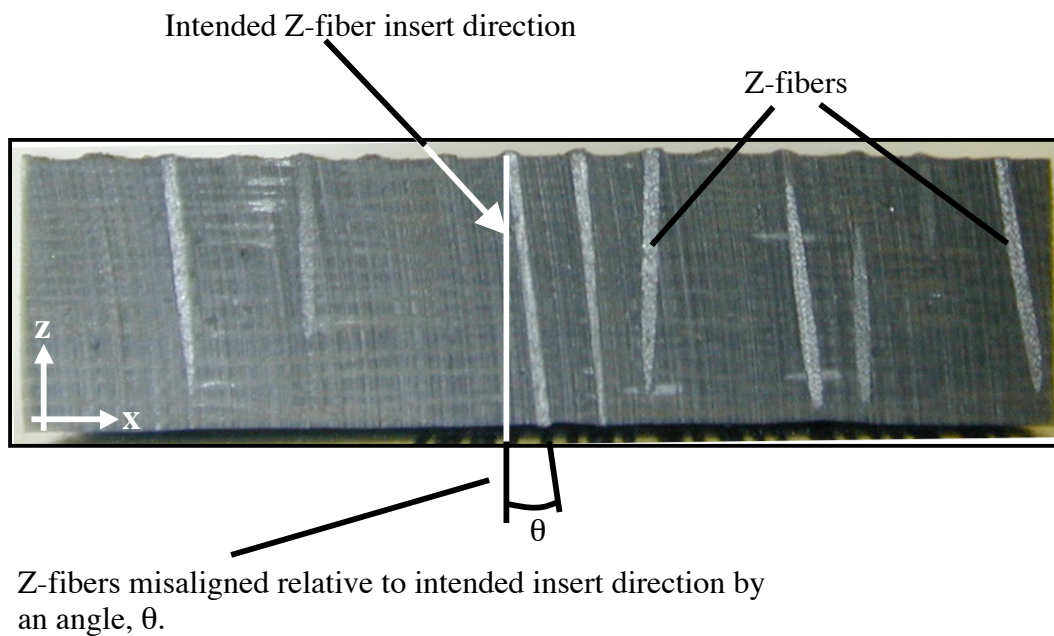


FIGURE 2. Cross-section of a laminate containing Z-fibers.

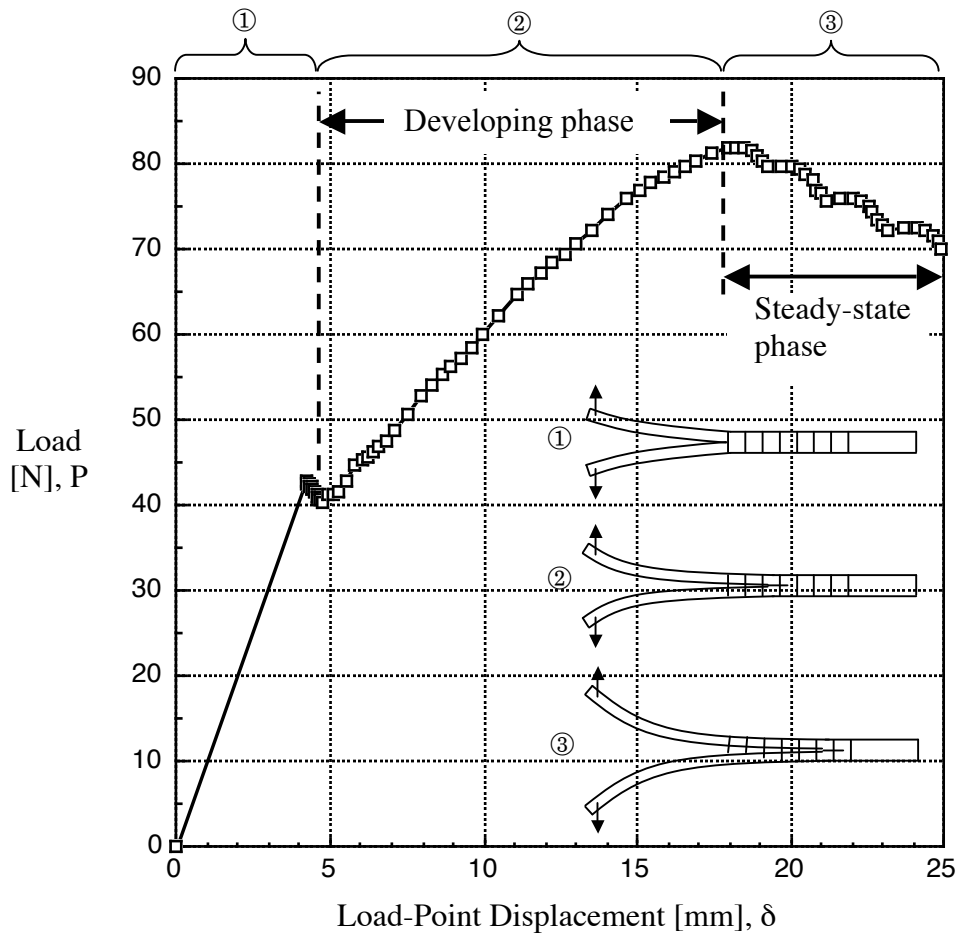


FIGURE 3. Load displacement response of DCB specimen reinforced with Z-fibers.

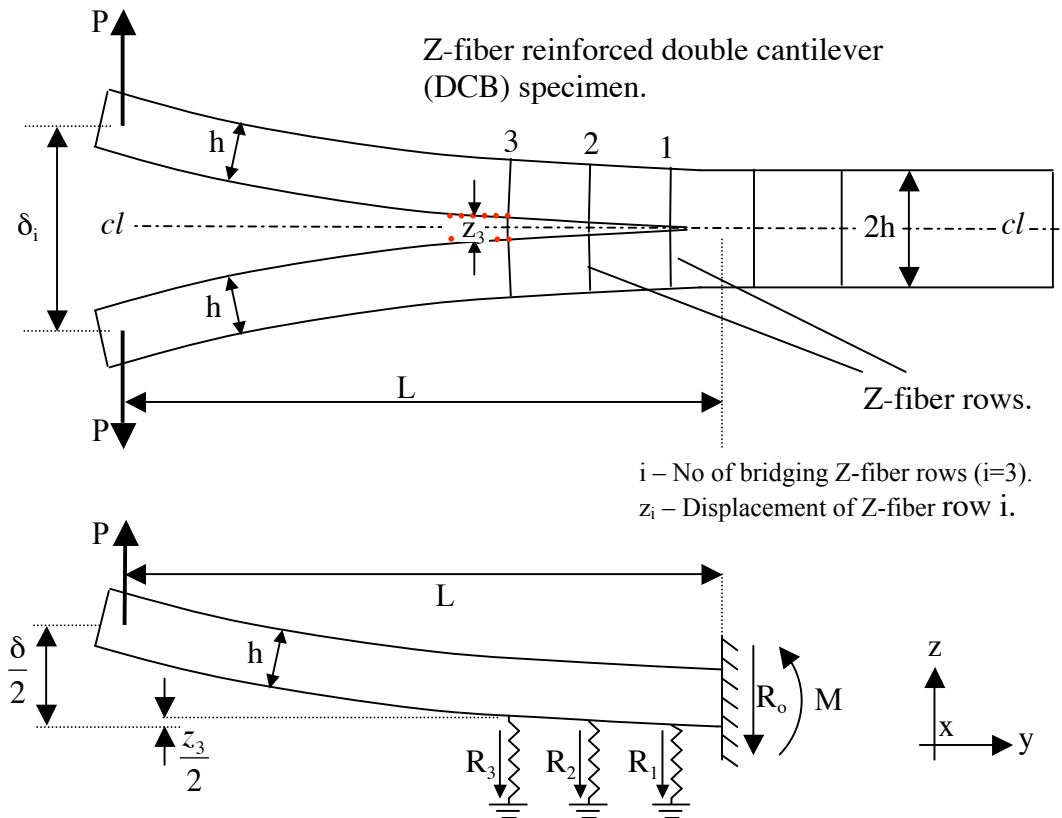


FIGURE 4. 2-Dimensional representation of Z-fiber reinforced DCB specimen.

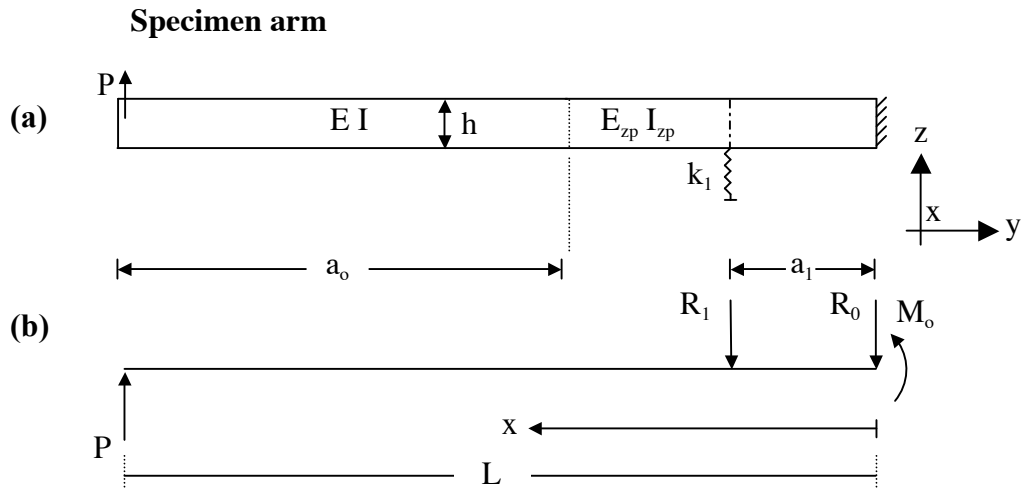


FIGURE 5. (a) Model of DCB specimen arm bridged by one Z-fiber row. (b) Free body diagram of the specimen arm.

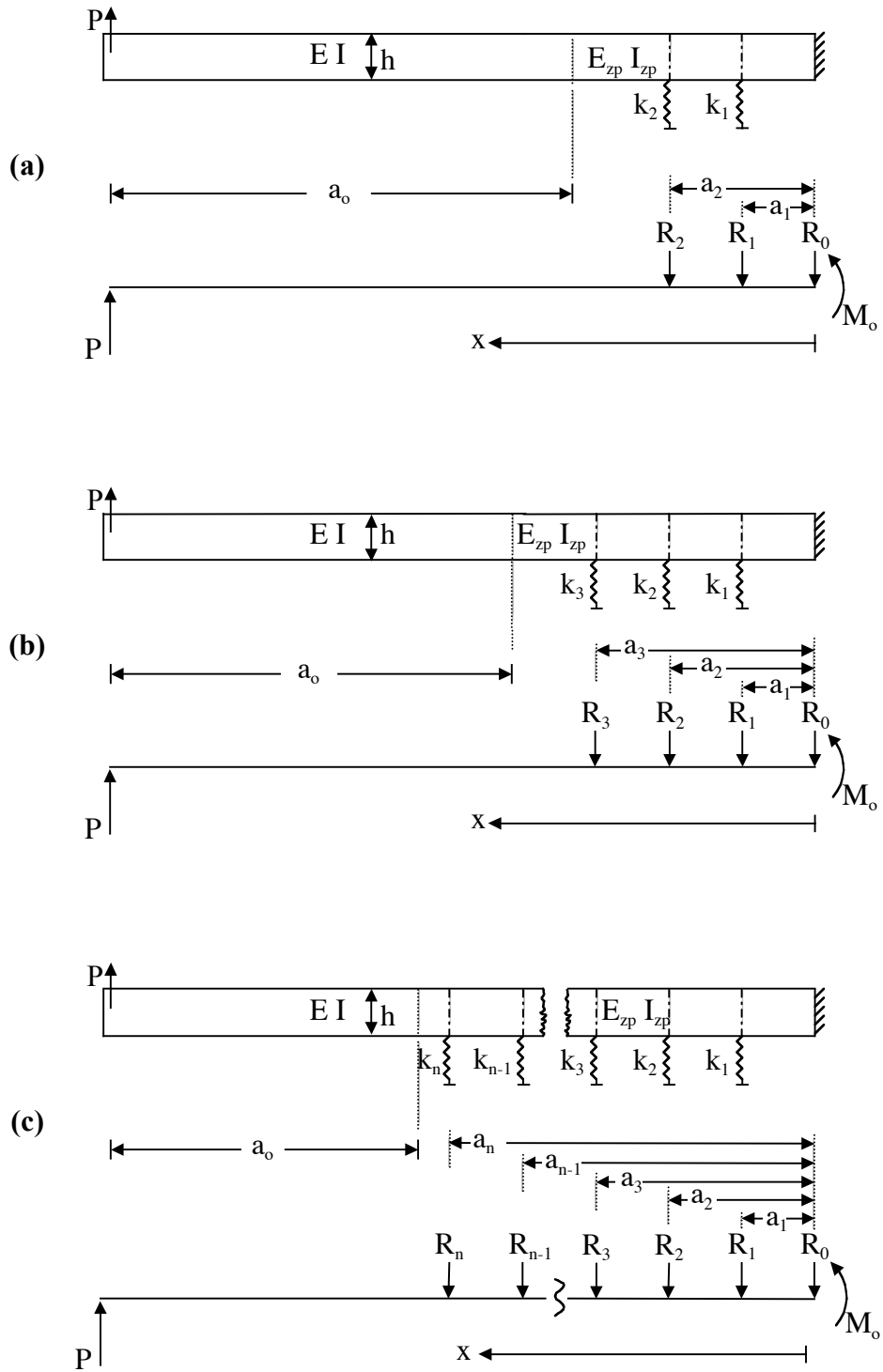


FIGURE 6. Models of DCB specimen arms bridged by: (a) Two Z-fiber rows, (b) Three Z-fiber rows, (c) Arbitrary number of Z-fiber rows,  $n$ .

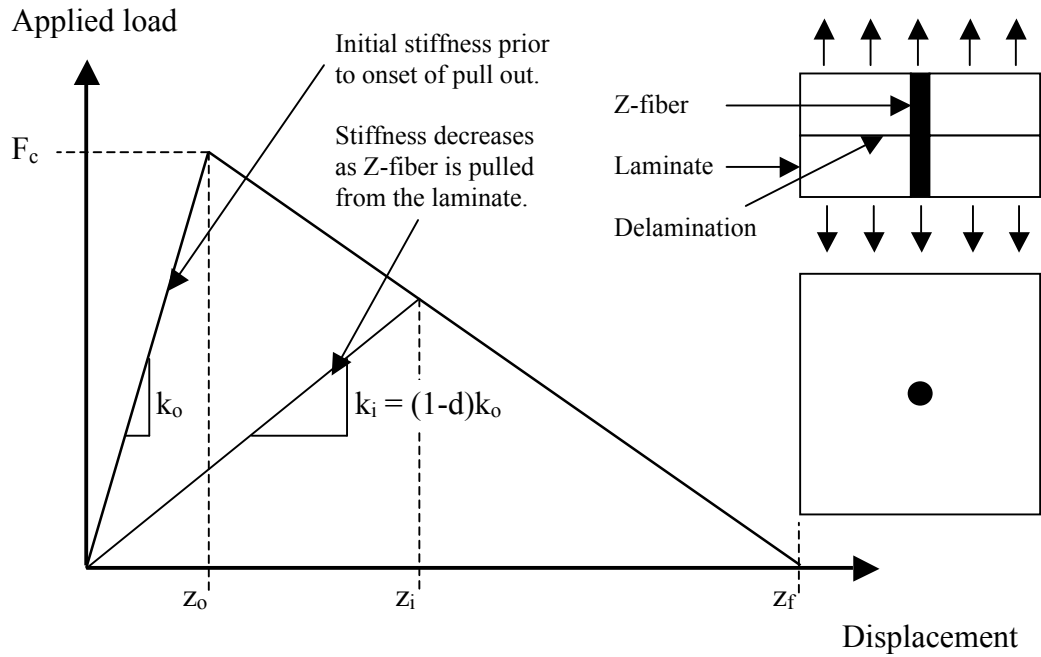


FIGURE 7. Idealized damage history of Z-fiber pull-out from a laminate. Illustration of single Z-fiber pull out test configuration.

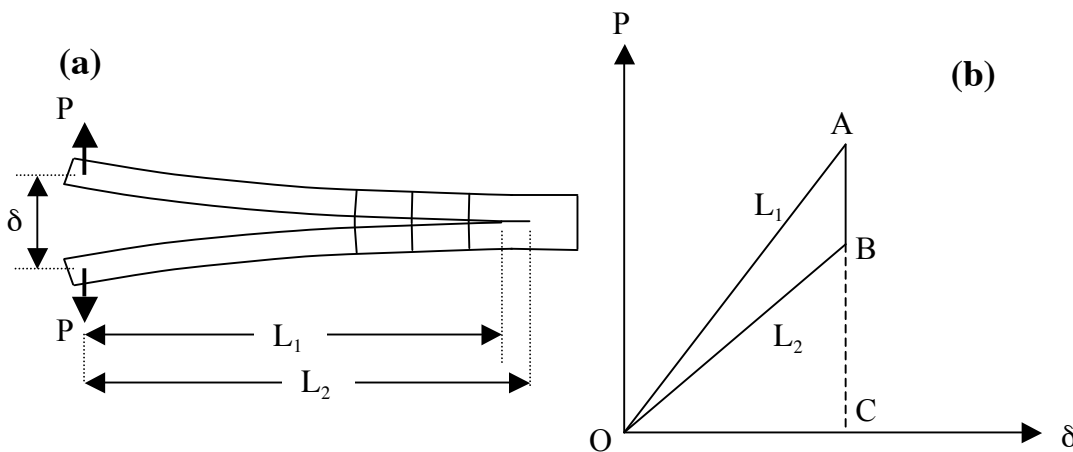


FIGURE 8. (a) Schematic of DCB specimen with two different delamination lengths. (b) Load displacement response of DCB specimen with different delamination lengths.

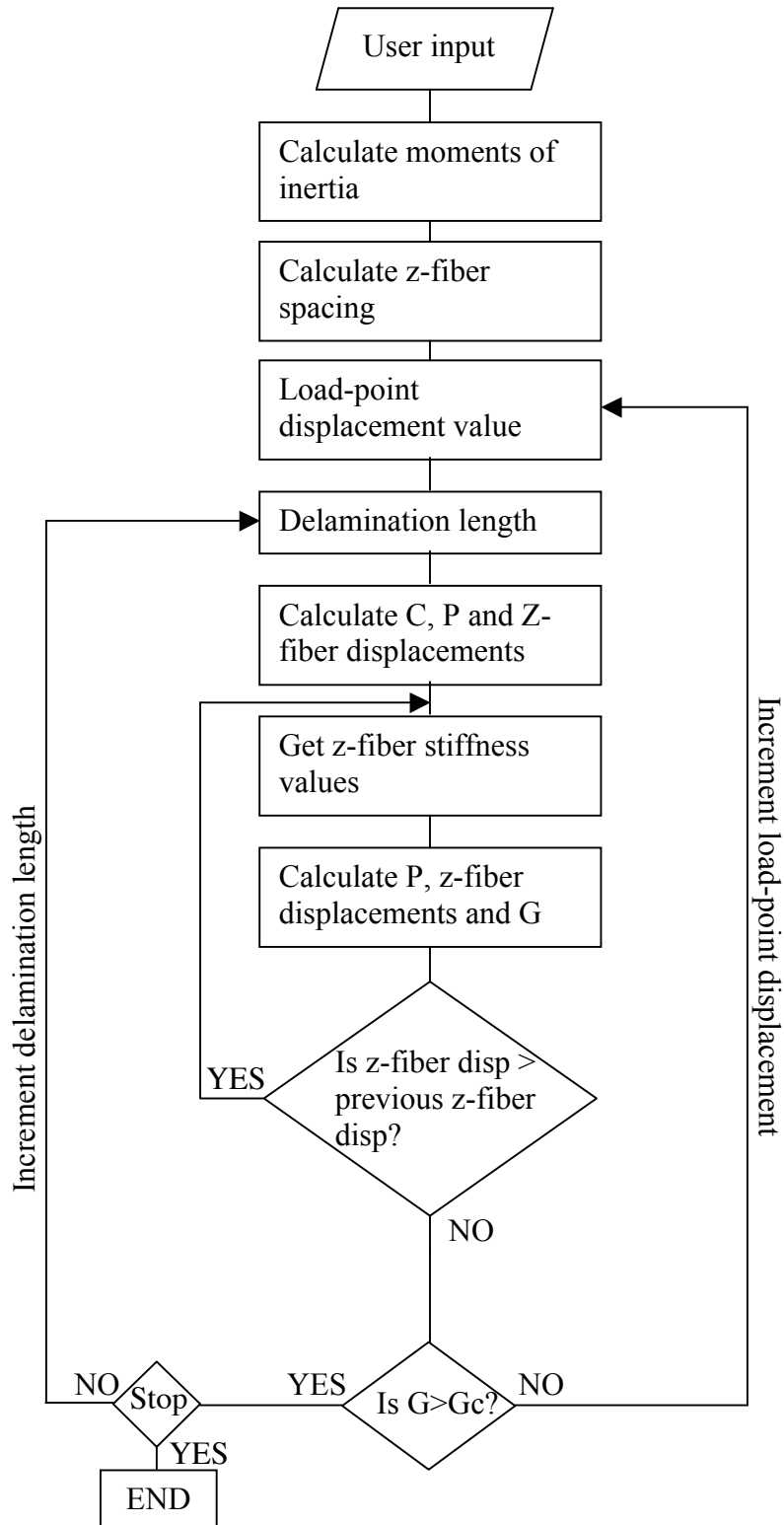


FIGURE 9. Flow chart of solution procedure for predicting delamination growth in Z-fiber reinforced DCB specimens.

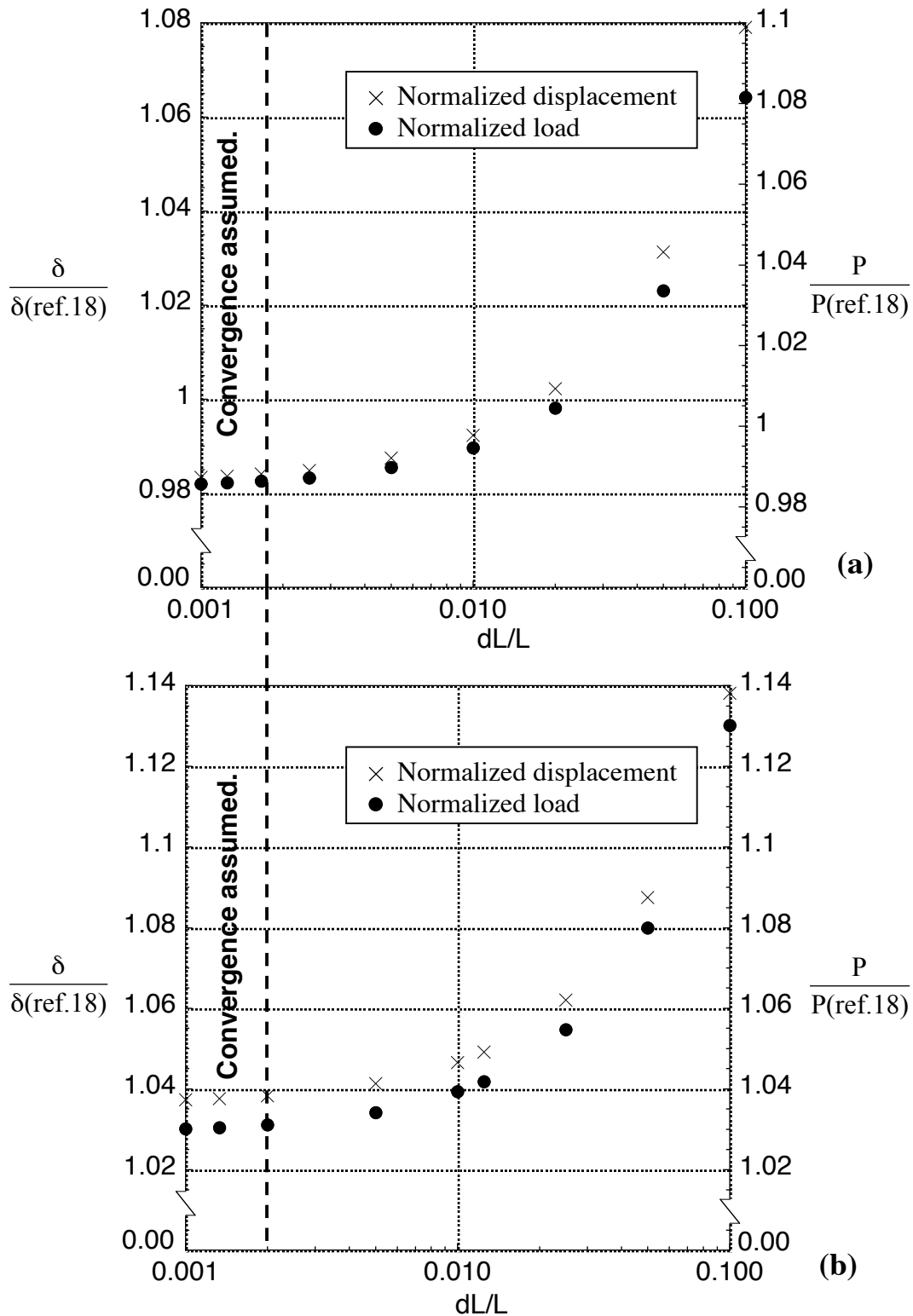


FIGURE 10. Load and displacement values as a function of  $dL/L$ , normalized by the corresponding experimental value. (a) Delamination length = 50mm. (b) Delamination length = 99mm [18].

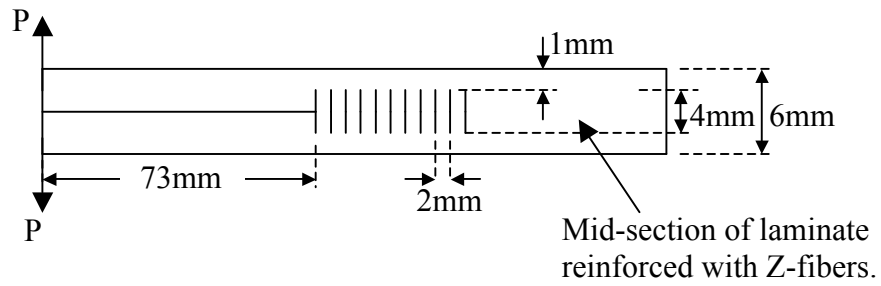


FIGURE 11. Specimen configuration used in Z-fiber reinforced DCB specimen investigation [12] (not drawn to scale).

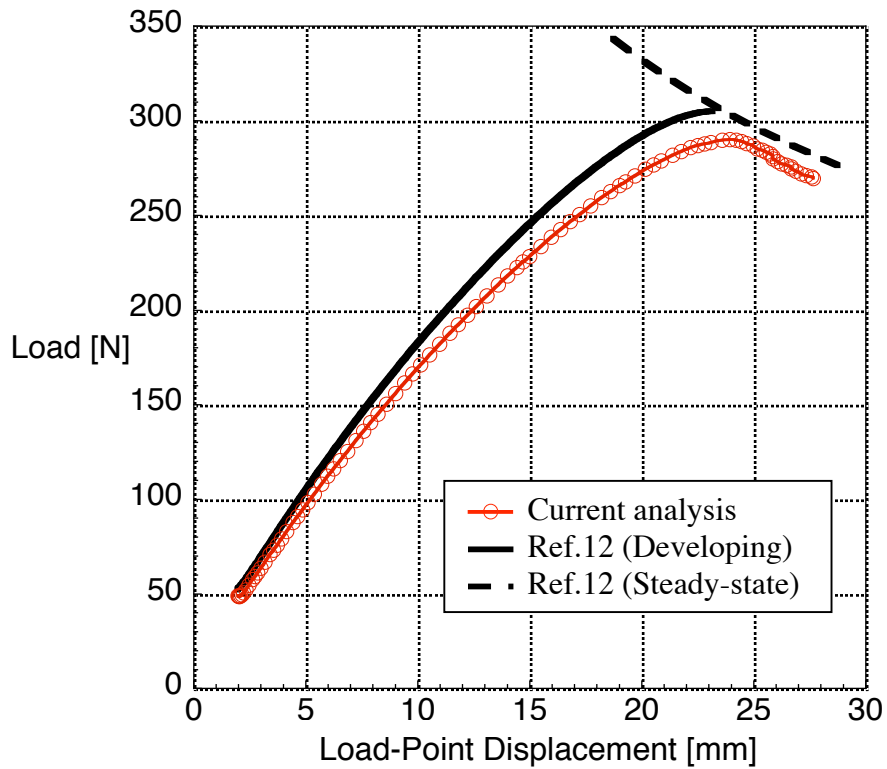


FIGURE 12. Estimated load displacement response of IM7/8552 DCB specimen containing 1.5% areal density of Z-fibers. Comparison with [12].

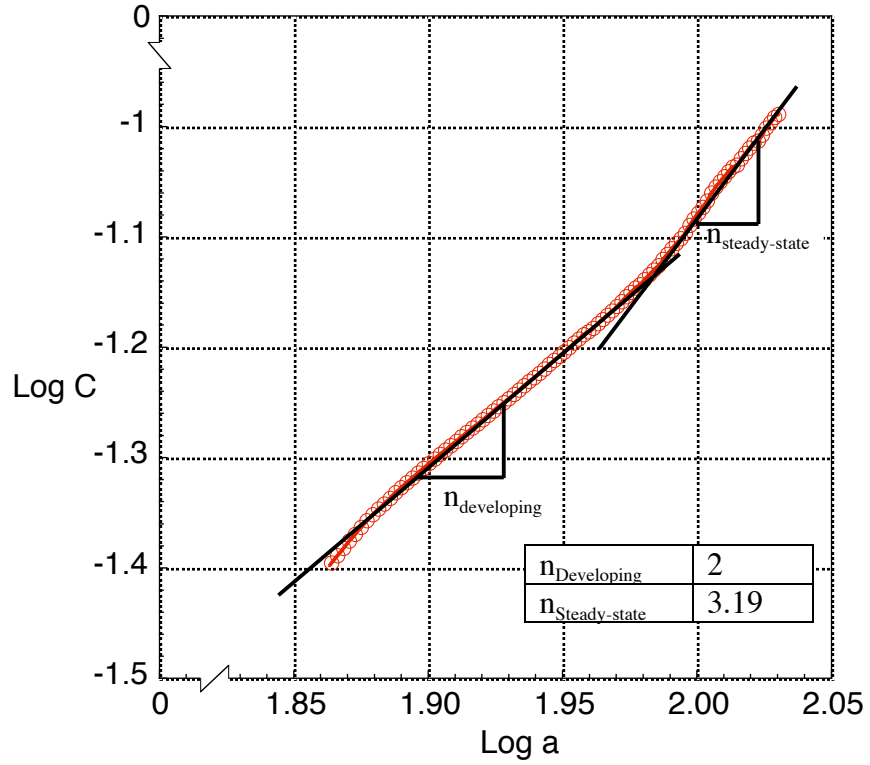


FIGURE 13. Compliance calibration plot from analysis of IM7/8552 DCB specimen containing 1.5% areal density of Z-fibers.

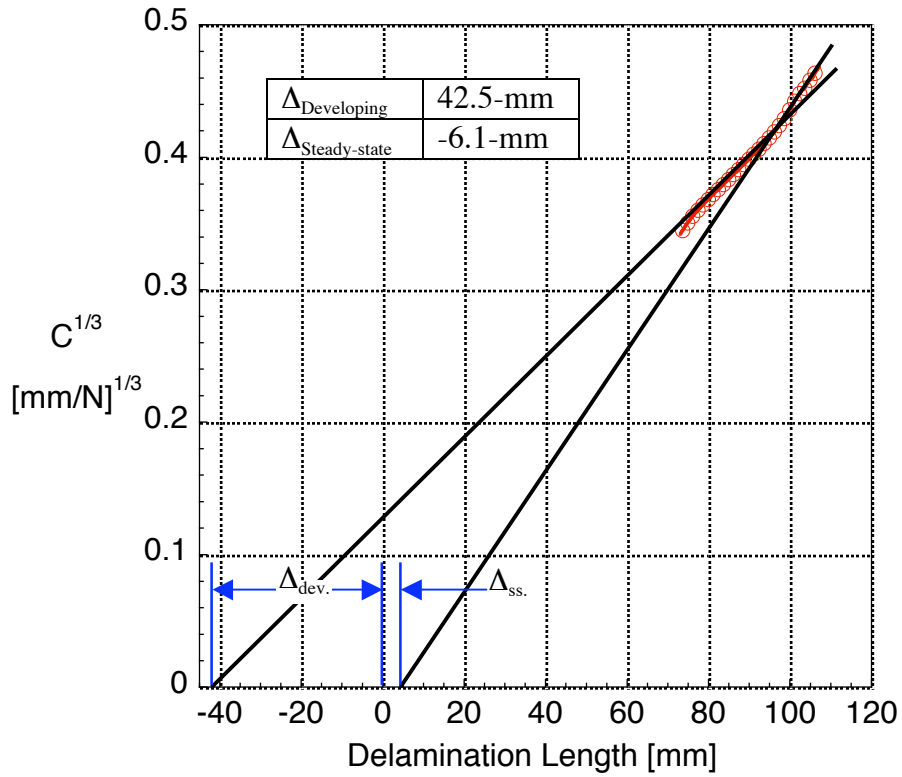


FIGURE 14. Modified beam theory plot from analysis of IM7/8552 DCB specimen containing 1.5% areal density of Z-fibers.

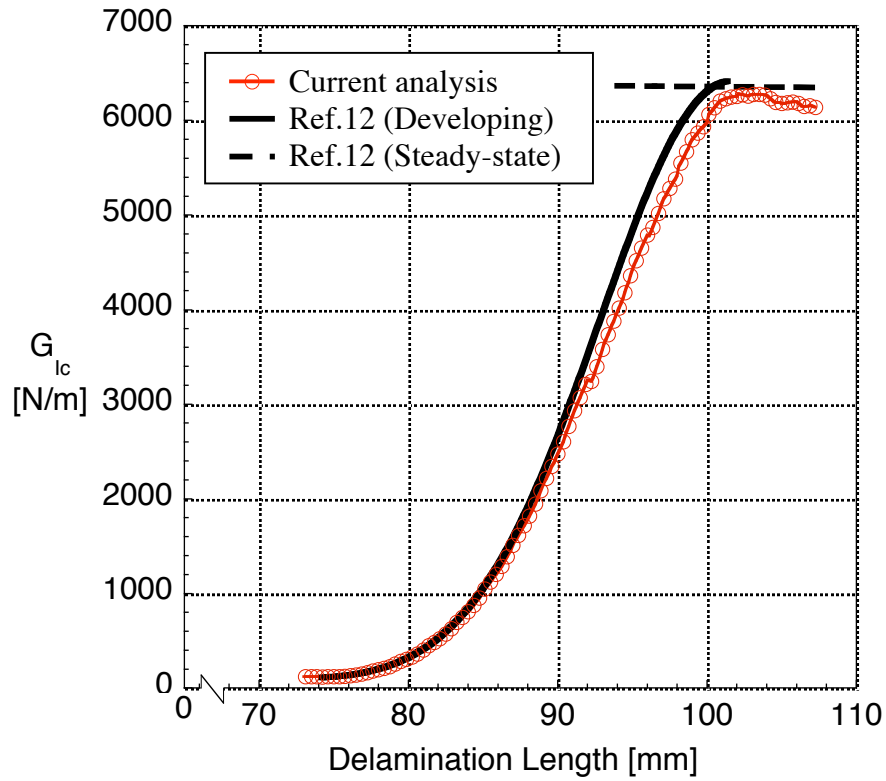


FIGURE 15. Estimated R-curve from analysis of IM7/8552 DCB specimen containing 1.5% areal density of Z-fibers. Comparison with [12].

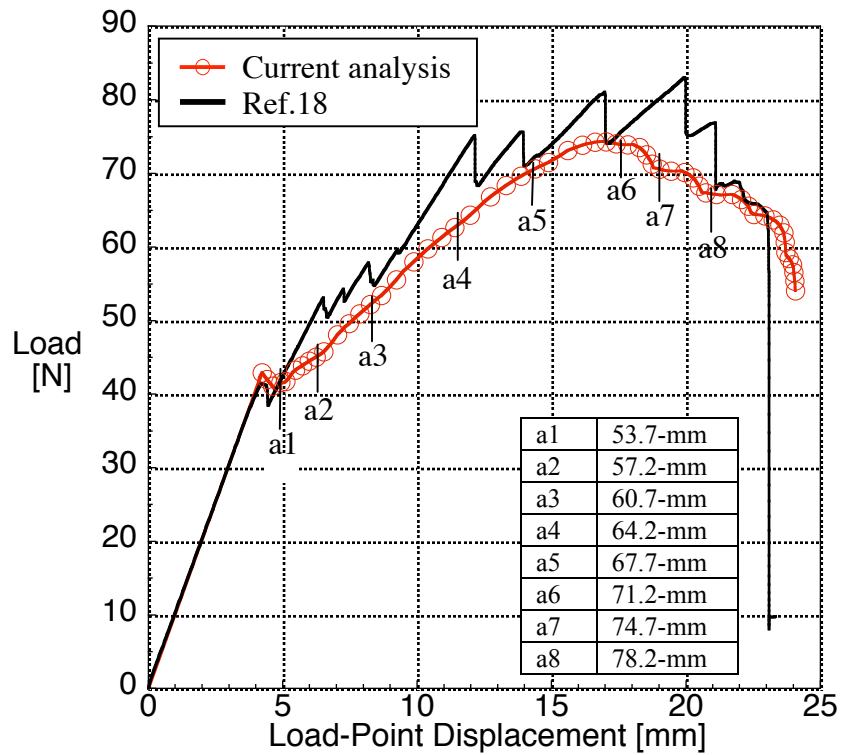


FIGURE 16. Estimated load displacement response of IMS/924 specimen containing 0.5% areal density of Z-fibers. Comparison with experiment [18].

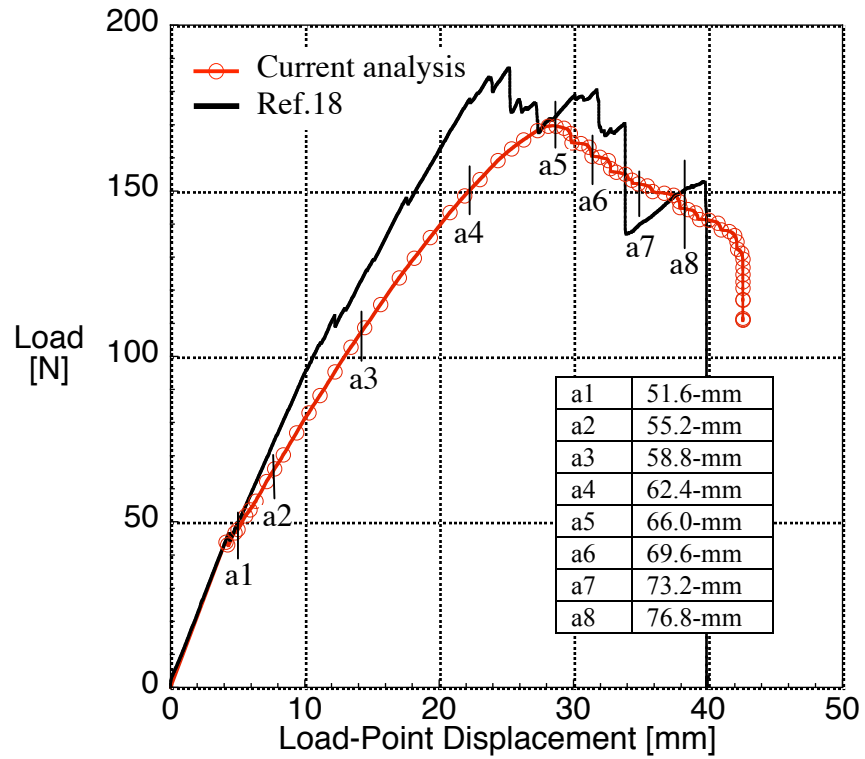


FIGURE 17. Estimated load displacement response of IMS/924 specimen containing 2% areal density of Z-fibers. Comparison with experiment [18].

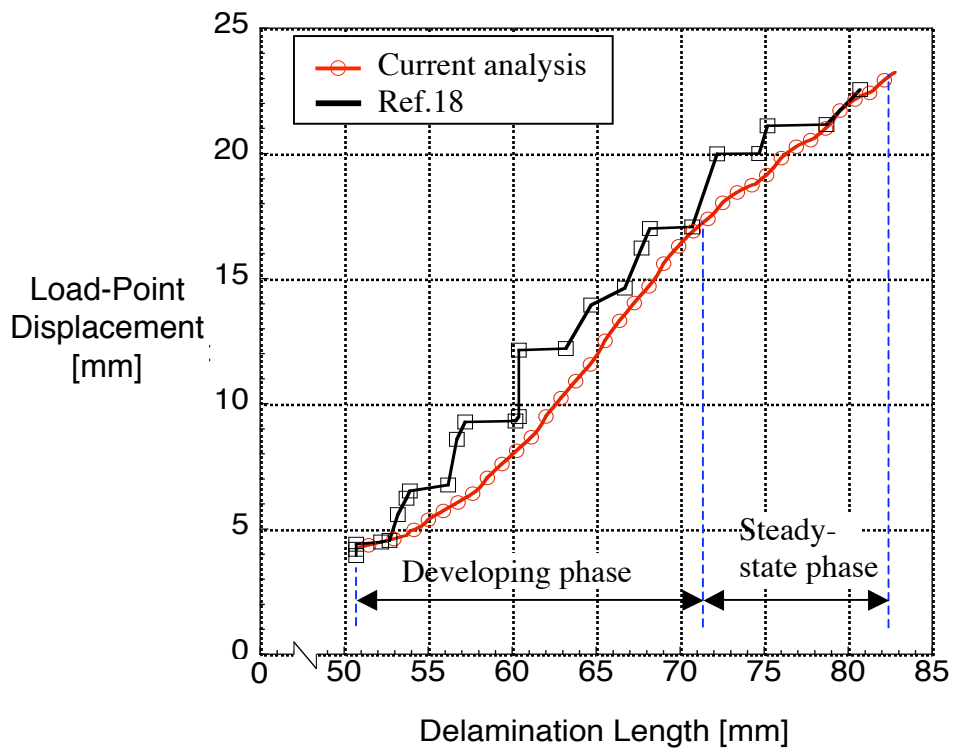


Figure 18. Displacement vs delamination length of DCB specimen with 0.5% areal density Z-fibers. Comparison with experiment [18].

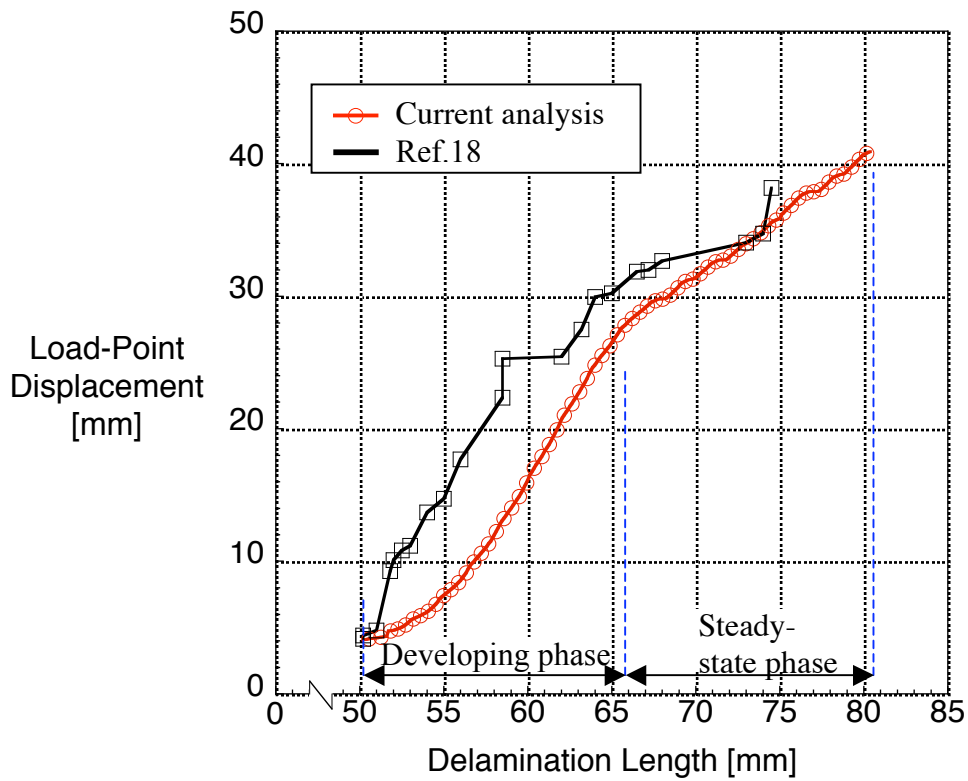


FIGURE 19. Displacement vs delamination length of DCB specimen with 2% areal density Z-fibers. Comparison with experiment [18].

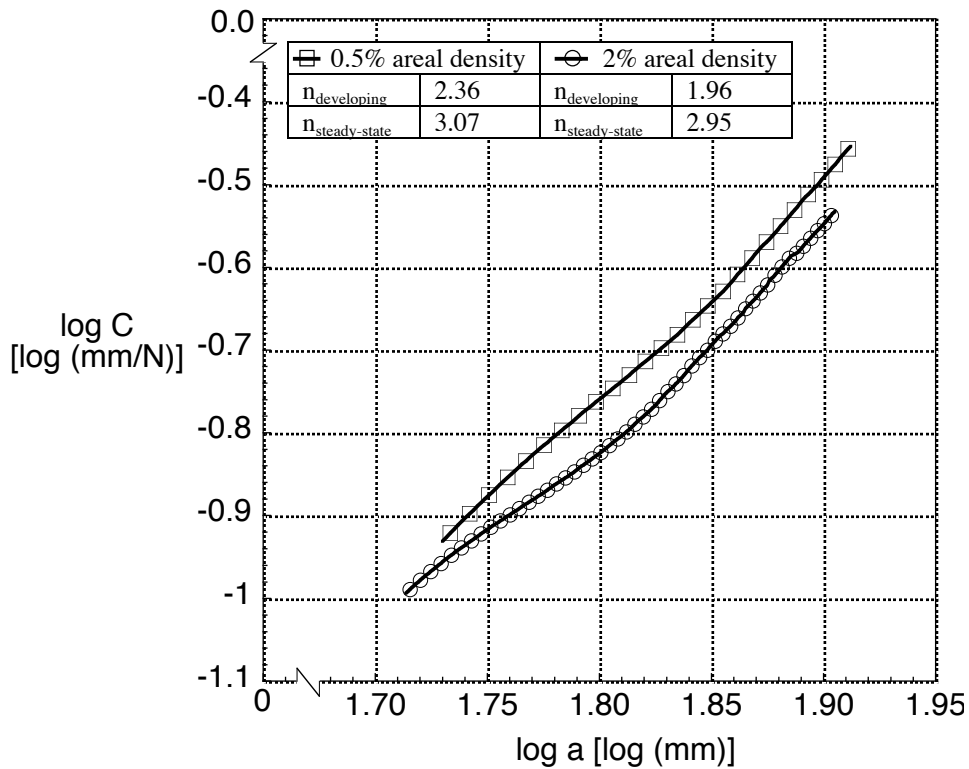


FIGURE 20. Compliance calibration plot from analysis of IMS/924 DCB specimen containing 0.5% and 2% areal density of Z-fibers.

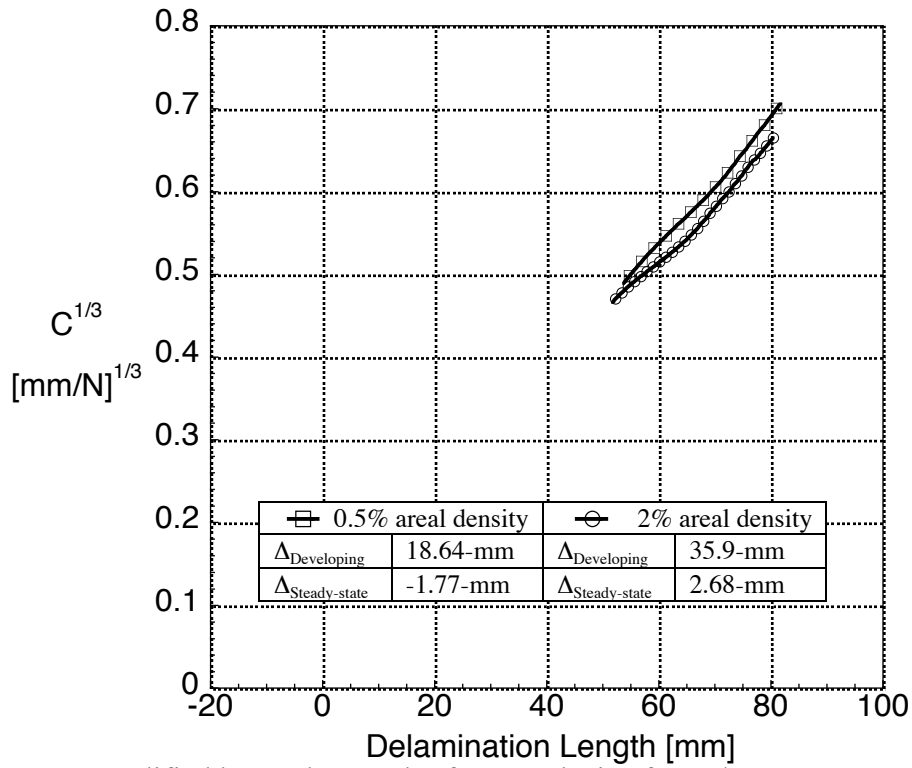


FIGURE 21. Modified beam theory plot from analysis of IMS/924 DCB specimen containing 0.5% and 2% areal density of Z-fibers.

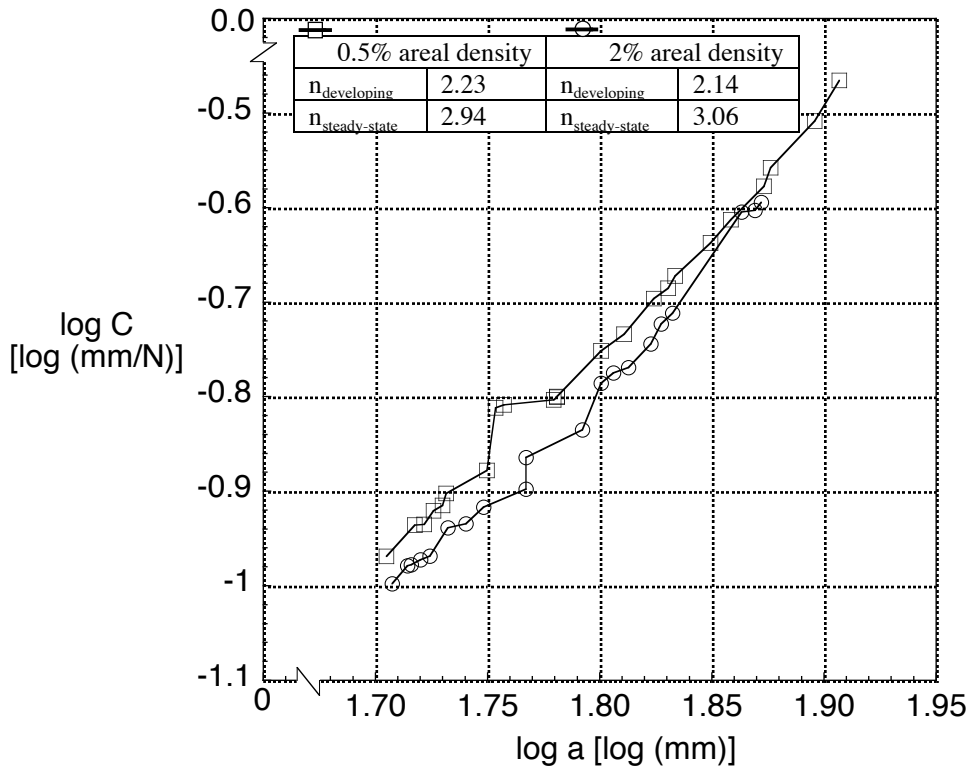


FIGURE 22. Compliance calibration plot using experimental test data [18] from tests on DCB specimens containing 0.5% and 2% areal density of Z-fibers.

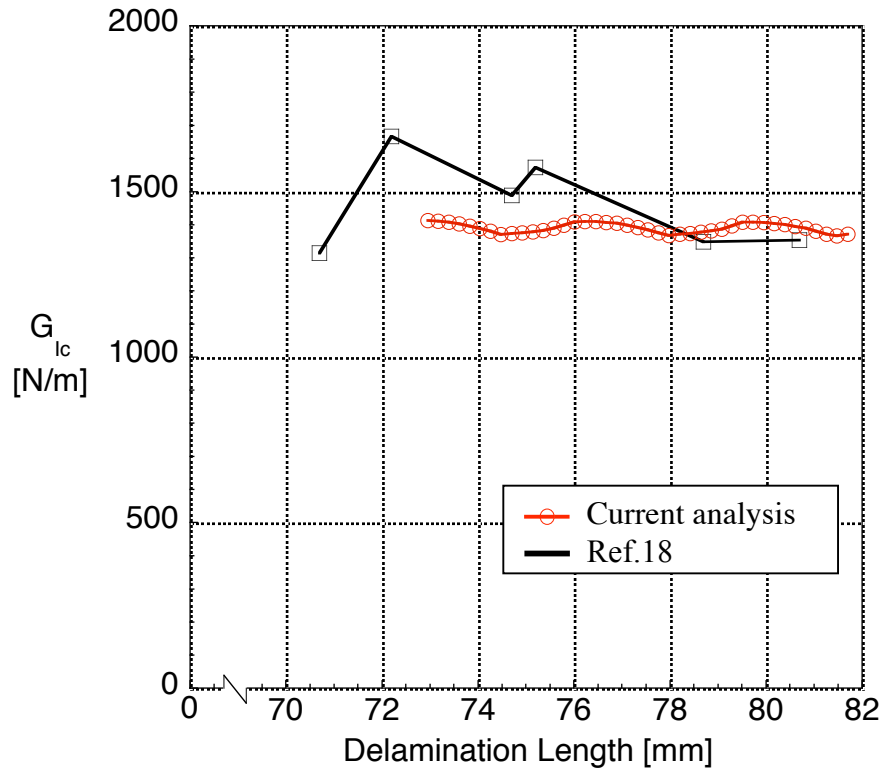


FIGURE 23. Estimated R-curve from analysis of IMS/924 DCB specimen with 0.5% areal density of Z-fibers. Comparison with experiment [18]

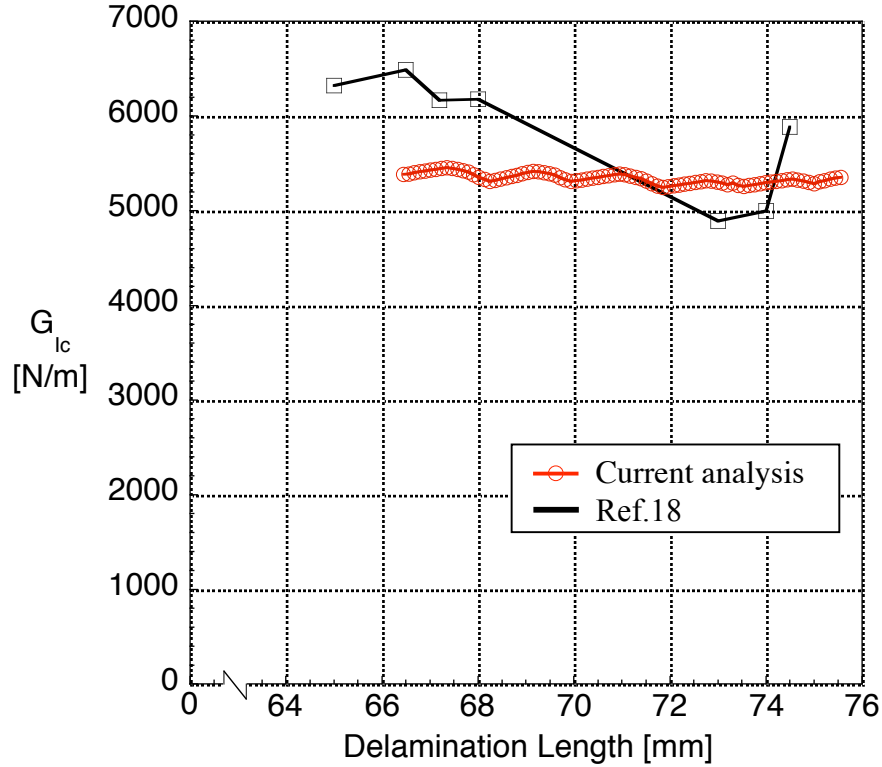


FIGURE 24. Estimated R-curve from analysis of IMS/924 DCB specimen with 2% areal density of Z-fibers. Comparison with experiment [18].

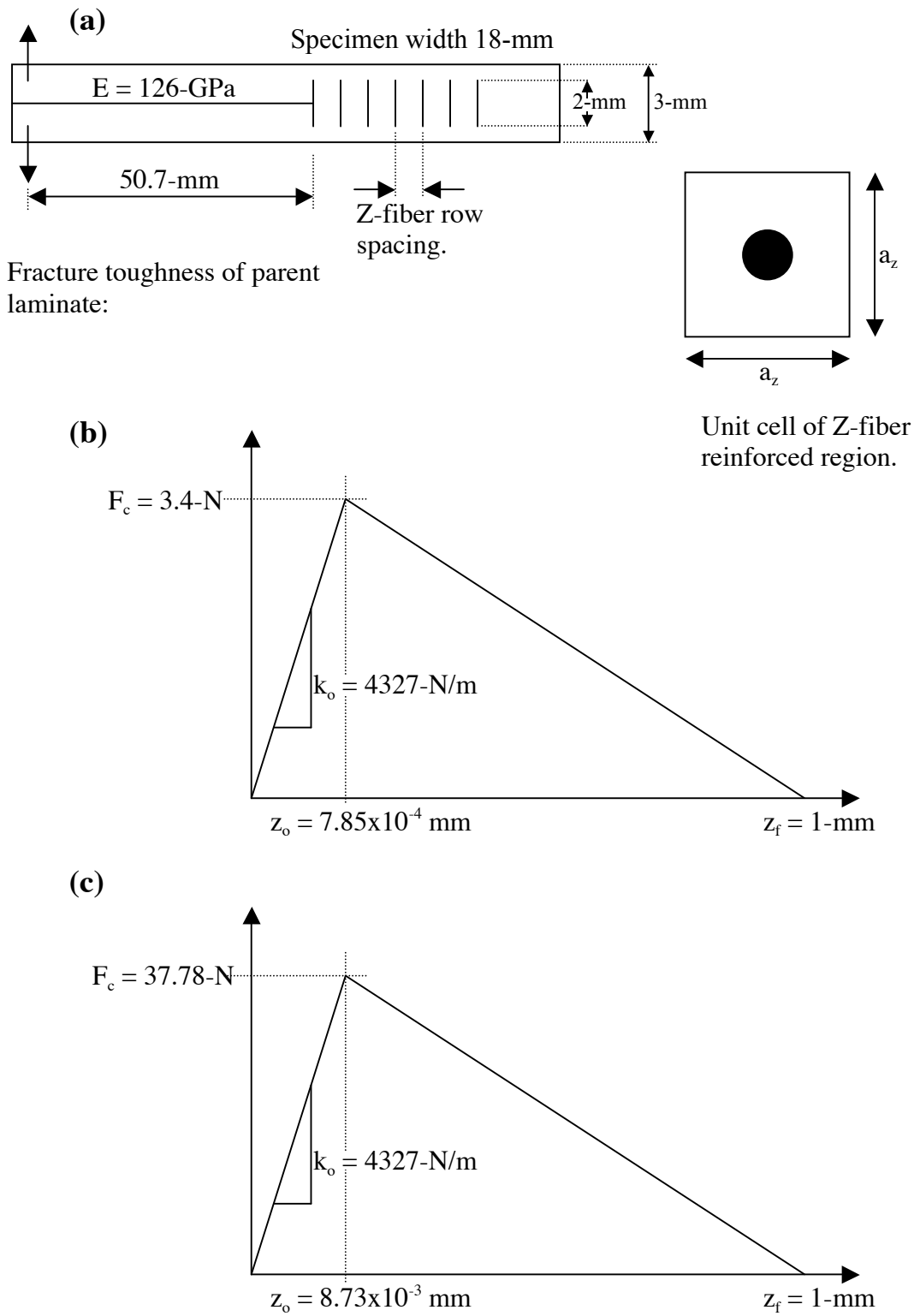


FIGURE 25. (a) DCB specimen modelled in Z-fiber row spacing study. (b) Bridging law for Z-fiber spacing case of 1.5-mm. (c) Bridging law for Z-fiber spacing case of 5-mm.

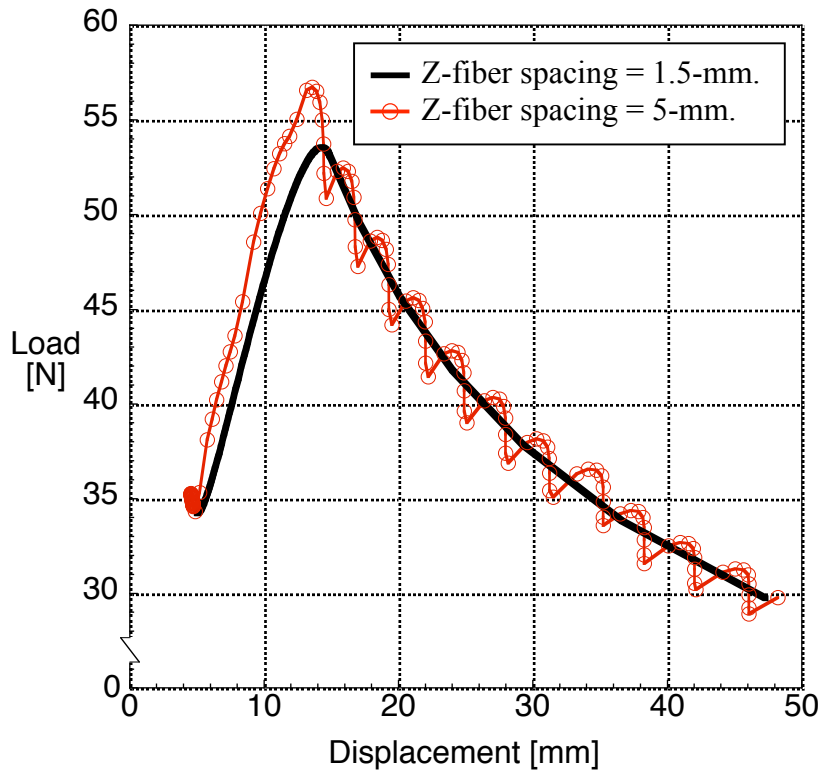


FIGURE 26. Load displacement response from analyses of DCB specimens with different Z-fiber spacing.

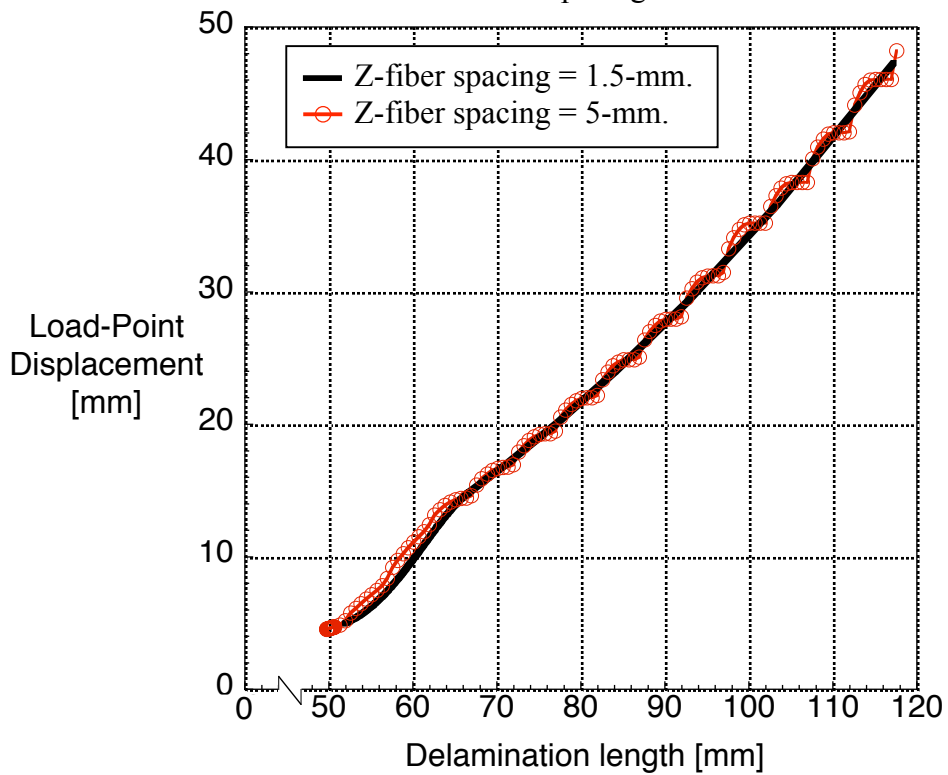


FIGURE 27. Load-point displacement versus delamination length curves from analyses of DCB specimens with different Z-fiber spacing.